ON A NOVEL METHOD OF INCORPORATING AN INTERNAL STRUCTURE INTO GREEN POWDER METALLURGY COMPACTS USING DIE COMPACTION

by

Geoffrey Beck

Submitted in partial fulfillment of the requirements
for the degree of Master of Applied Science

at

Dalhousie University
Halifax, Nova Scotia
August 2012

DALHOUSIE UNIVERSITY

DEPARTMENT OF MECHANICAL ENGINEERING

The undersigned hereby certify that they have read and recommend to the Faculty of Graduate Studies for acceptance a thesis entitled "ON A NOVEL METHOD OF INCORPORATING AN INTERNAL STRUCTURE INTO GREEN POWDER METALLURGY COMPACTS USING DIE COMPACTION" by Geoffrey Beck in partial fulfillment of the requirements for the degree of Master of Applied Science.

Dated: August 2, 2012

Supervisor: _____

Reader: _____

Reader: _____

DALHOUSIE UNIVERSITY

DATE: August 2, 2012

AUTHOR: Geoffrey Beck

TITLE: On a Novel Method of Incorporating an Internal Structure into Green Powder Metallurgy Compacts using Die Compaction

DEPARTMENT OR SCHOOL: Department of Mechanical Engineering

DEGREE: M.A.Sc. CONVOCATION: October YEAR: 2012

_____

Signature of Author

To my friends and family

TABLE OF CONTENTS

LIST OF TABLES

LIST OF FIGURES

ABSTRACT

A novel method of producing die compacted powder metallurgy components with fully enclosed internal structures was developed. The physical characteristics of the compacts were evaluated by measuring bulk density, internal density gradients and compressive green strength. Additionally, a finite element simulation was developed to evaluate the compaction process of the internal structure compact.

The internal structure compact displayed the anticipated lower bulk densities due to the less dense internal structure than a conventional powder metallurgy compact, however; higher local densities were found within the internal structure compact at all compaction pressures. Compressive green strength characteristics showed unique results where the strength increased up to 300 MPa compaction pressure, however; at 400 MPa there was a distinct plateau in green strength. This phenomenon was attributed to an increase in differential shear stress around the internal structure with a minimal increase in density from 300 MPa to 400 MPa.

List of Abbreviations and Symbols Used

Abbreviation	Description
PM	Powder metallurgy
CIP	Cold isostatic press
HIP	Hot isostatic press
SS	Stainless steel
CAl	aluminum 356 casting alloy
LC	Low carbon steel
BCC	Body centered cubic
FCC	Face centered cubic
CT	Computed tomography
LVDT	Linear variable displacement transducer
D	Compact diameter
h	Compact height
K	Ratio of top and bottom compaction stresses
F_N	Normal force
F_S	Shear plate force
CGS	Compressive Green Strength

Greek Symbol	Description
ϱ_g	Green density of test cylinder
σ_{zt}	Top punch compaction pressure
σ_{zb}	Bottom punch compaction pressure
σ_z	Average compaction pressure
σ_r	Radial die wall stress
μ	Coefficient of friction

ACKNOWLEDGEMENTS

There are many people that I would like to thank, for without them this body of work would not have been possible:

Cecilia Newton for her unwavering support and encouragement. Stanley Selig, for his help, assistance and the occasional distraction. Dr. Darrel Doman for his guidance, patience, and for providing me with the opportunity to pursue graduate studies. Dr. Paul Bishop and Randy Cooke; for the use and instruction in the PM lab. Braden Murphy, and Carmen McKnight and all the other members of the T-Building for making this a memorable two years. Dr. Kevin Puckett, for the use of his microscope and image software. And finally all of the staff and faculty of the Department of Mechanical Engineering.

Thank you.

Chapter 1: INTRODUCTION

Internal structures are part inserts in components which serve to provide a practical benefit to the design, operation, and fabrication of mechanical and structural components. Perhaps the most well-known internal structure is reinforced concrete in which concrete completely surrounds the rebar. The rebar serves to increase the tensile strength of the concrete, which otherwise would suffer from poor tensile strength and thus greatly limit its applications. In addition to reinforcing concrete, internal structures are contained within parts for various reasons, including; altering strength and mechanical properties; such as radial tires that contain steel belts that increase tire strength and also help maintain tire shape. Furthermore, weight and material savings can be gained from internal structures; BMW vehicles employ lightweight aluminum control arms that are manufactured by vacuum riserless casting/pressure riserless casting (VRC/PRC) methods around a hollow internal structure. The final product is a metal composite component consisting of two distinct components: the solidified aluminum exterior and the enclosed hollow internal structure (Aluminum Association, 2008). However, the manufacture of metal composite components suffers from several technical and economic challenges. Typically, high energy and multi-step processes are required, resulting in high production costs and low production cycle times.

The above challenges associated with manufacturing internal structure components present a unique opportunity to leverage the benefits of the powder metallurgy (PM) press-and-sinter technique with those of bodies with internal structures. The press-and-sinter technique involves pressing (compacting) powder in a rigid die under high pressure to form a so-called

green compact. The green compact is then heated at elevated temperatures under a controlled atmosphere (sintering).

In the previous reinforced concrete example; the internal structure (rebar) must be properly encased in the concrete matrix in order to achieve optimal strength characteristics. As a result, the manufacturing method is one where significant labor is required in addition to multiple steps. However, if an encased internal structure were able to be manufactured in a single step, significant cost savings could be realized. Furthermore, die compaction; which is the first stage of the press-and-sinter technique described above; results in low material wastage and minimal secondary machining operations, this serves to further reduce the cost.

The objective of this work is to develop a novel method of incorporating an internal structure into PM components using die compaction. Specific emphasis is placed on the production of PM non-heat treated (green) cylindrical powder compacts (diameter D, height H) with spherical structures (sphere diameter d, wall thickness t) fully enclosed within a powder matrix, as is shown in Figure 1. These compacts are more easily stated as internal structure compacts; which is comprised of a PM matrix (powder), a cavity shell (spherical structure) and a cavity fill. The development of the compacts will be constrained to cylindrical green compacts and thus, sintering will not be a main focus of this work.

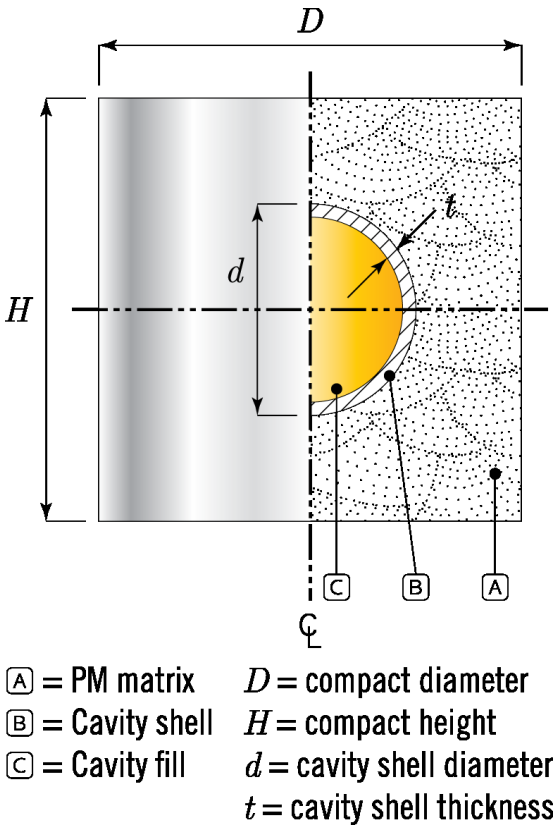

Figure 1: A section view of the internal structure compact illustrating the internal structure (B), structure fill (C) and the powder matrix (A).

Chapter 2: POWDER METALLURGY BACKGROUND

PM is an alternative manufacturing technology in which powdered metal is consolidated into a desired shape or component. One of the most common PM processing techniques is the press-and-sinter approach, widely used in a variety of high-volume, low-cost operations. Powder is first pressed (compacted) in a rigid die under high pressure to form a so-called green compact. Green compacts are very near the final desired shape (near-net-shape) but are characterized by incomplete densification of the powder. That is, the bulk density of the part is lower than the theoretical full density of the solid metal. To set the internal microstructure, thereby setting the mechanical strength, green compacts are heat treated at elevated temperatures (sintering).

There are numerous advantages of PM techniques over its conventional counterparts:

- Minimal raw material wastage.
- Minimal secondary machining required.
- High-volume, low-cost production capabilities.

Compared to other processes such as casting, chip generating machining (*e.g.* grinding, milling), forging and extruding; PM techniques offer considerable advantages in terms of material utilization and energy demands. Dale (2011) undertook a study which quantified the amount of raw material remaining in a part as well as how much energy is consumed per kilogram of produced part. His results, summarized in Figure 2, clearly show that PM has much less material wastage and lower overall energy demands compared to competing processes. It should be noted that while the deep drawing processing technique is comparable in performance it is limited to sheet metal raw materials.

Maximizing material utilization (equivalently minimizing raw material wastage) has obvious direct cost benefits but there are other cost savings realized through PM processes. In titanium alloy aerospace applications the raw alloy in ingot form costs four times more than high strength steels and using PM titanium alloys results in a 40% cost savings on raw materials (Fang, 2010).

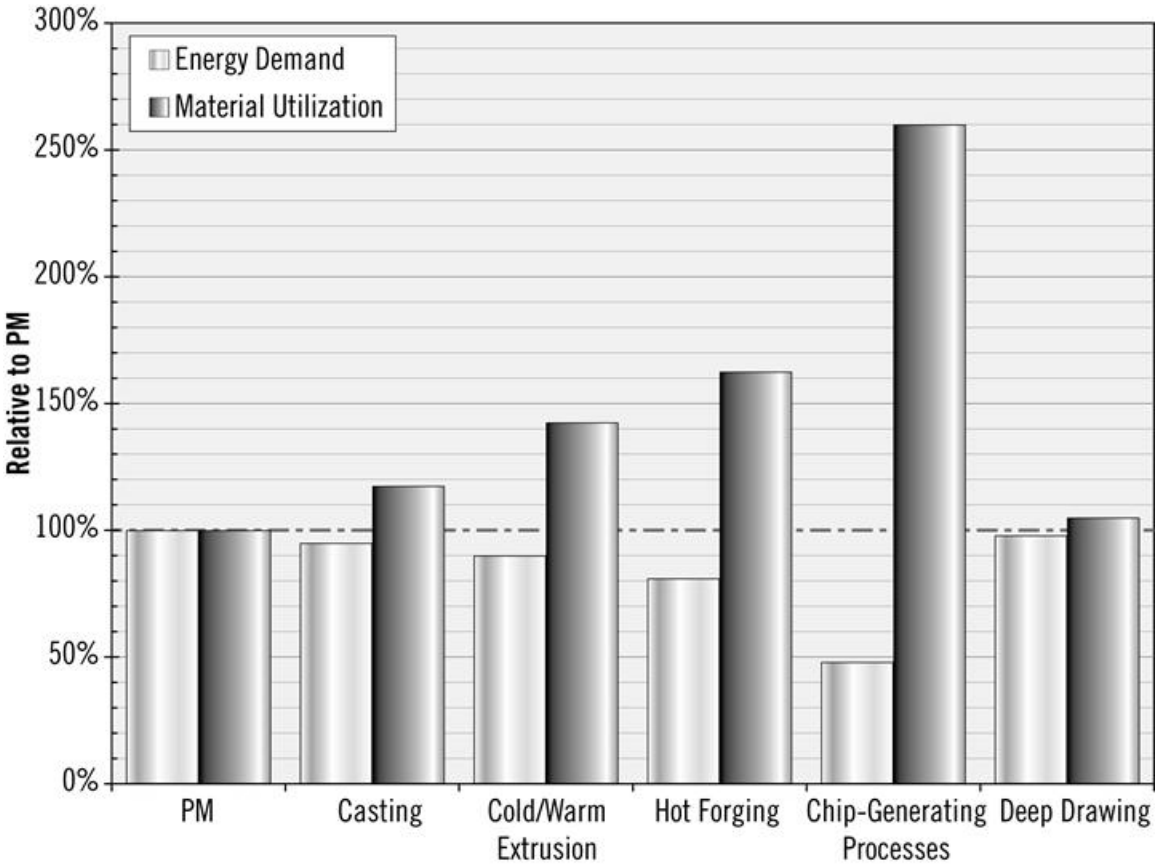

Figure 2: PM comparison of material utilization and energy demand of other processes.

The automotive industry, PM's largest consumer, enjoys similar raw material costs savings but its primary benefit is the significant costs savings derived from the lack of secondary machining required. Common engine components, such as connecting rods, are now manufactured on a large scale with drastically reduced manual metal-forming (Donaldson, 2011). While PM parts have been used extensively in automobiles for over a decade, recently their use has increased markedly. The average American-made vehicle used an average of 19 kg

of PM parts in 2010 and is ever-increasing with the 2011 Ford Edge containing 30 kg of PM product (Lutheran, 2011). Furthermore, the surge in hybrid and electric vehicles in the automotive marketplace makes PM technologies ideally situated to make an impact using lightweight alloys (Capus, 2011). Conventional manufacturing methods make the extensive use of aluminum in vehicles prohibitive but the high-volume; low-cost PM route offers an attractive alternative in which manufacturers can implement lightweight designs with marginal cost increase.

2.1 Powder Production Methods

Currently, there are three broad categories of manufacturing metal powder that are employed by the PM industry: physical, mechanical, and chemical. Within each category there are various sub-methods:

- Physical: gas, water, and centrifugal atomization.
- Mechanical: machining, milling, and mechanical alloying.
- Chemical: decomposition of a solid by a gas, electrolytic production, and thermal decomposition.

The selection of the production technique depends on several factors such as: desired chemical or physical characteristics (shape & size), powder quality, and the economic climate (Meluch, 2009).

2.1.1 Physical Production

Physical production techniques are generally comprised of (but not limited to) gas, water, and centrifugal atomization. Gas and water atomization involve obliterating a stream of molten metal using gas (N_2, Ar, He, Air) or water into fine particles that solidify into powder particles. This process can be applied to any metal or alloy that can be melted; however, reactive metals such as Al, Mg, Ti, Zr are only compatible with gas atomization. Water atomi-

zation generally yields more irregular powder morphology with a relatively large powder particle size (approximately 150 μm) (German, 2005). Similarly, employing air also produces an irregular powder morphology shape with a similar powder particle size. Inert gas atomization (N_2, Ar, He) generally yields a more spherical powder morphology with a relatively small powder particle size (approximately 100 μm) (German, 2005). Atomization is the most dominant powder production method currently employed by the PM industry because of favorable economics and high production rates.

2.1.2 Mechanical Production

Mechanical production consists of three facets: machining, milling and mechanical alloying. Machining, as the name suggests, consists of turning or grinding solid stock into a powder; usually with a curled morphology. The drawback of this production method is machining fluid contamination and work hardened particles that yield poor compaction characteristics.

Milling is the most popular mechanical production technique; it produces powder by applying impact (*e.g.* ball mill) to a coarse material feed. The major requirement of this method is the feed material must be brittle; otherwise the feed will not be fractured into smaller particles. Therefore, the feed is often manipulated into a brittle form (hydration) pre-milling, and after milling this process is reversed to restore material ductility.

Mechanical alloying is a combination of grinding, milling and alloying into a single step. This process employs a raw powder mixture as the feed in a ball mill. The benefit of this process is that compressive load induces alloying, work hardening, and particle fracture in a cycle. This can result in a very fine grain size which gives excellent mechanical properties in the final PM product.

2.1.3 Chemical Production

There are two main types of chemical production: decomposition of a solid by a gas and electrolytic production. Decomposition of a solid by a gas is a chemical production technique that is often employed for Fe, Mo, W and Cu powders, and, it is virtually the sole method used to produce refractory powders (W, Mo). This is because the respective melting temperatures of W and Mo are too high to produce powders with more conventional techniques such as atomization. The chemistry behind the process involves the reduction of metal oxide into a metallic form by way of CO or H_2 as the reducing agent. The final powder product has a spongy morphology that is characterized by internal porosity.

Electrolytic production is used to produce elemental powders from an initially solid purified metallic plate. The plate is used as the anode of an electrochemical cell. A current is passed through the anode to a cathode by way of an electrolyte. This process causes the initial plate to be dissolved and then precipitated on the cathode. The precipitated metal is finally ground into a powder which usually has dendritic morphology (Cu, Ag) or an angular morphology (Fe, Mn, Co).

2.2 Powder Form

There are two powder forms that can be used in PM process; elemental and pre-alloyed powder. Elemental powder is a mix of various elements in powder form that are combined to create the desired alloy when sintered; for example, a mix of copper and tin powders will form bronze when sintered. Conversely, pre-alloyed powder is defined as each powder particle being in the form of the alloy in question. Generally, as elemental metals are softer than their alloys, elemental powders yield higher green densities and have better compaction characteristics than their pre-alloyed equivalent (German, 2005).

2.3 Compaction Methods

There three main forms of powder compaction that are utilized in the PM manufacturing industry: Uniaxial die compaction, cold isostatic pressing, and hot isostatic pressing. There are many other methods of powder forming; however, this report will focus the three methods listed above as they are the most common in industry.

2.3.1 Cold Isostatic Pressing

Cold isostatic pressing (CIP) is performed by applying compaction pressure to the powder via pressurized fluid that is maintained at approximately room temperature. The powder is contained in a flexible form in the shape of the desired part. The benefit of the CIP is that the finished part has a highly uniform density distribution, however; it is a slow process that results in poor dimensional tolerances, which consequently require additional secondary machining processes.

2.3.2 Hot Isostactic Pressing

Hot isostactic pressing (HIP) is involves pressing powder in a sealed glass or metal container at elevated pressures and temperatures. The container deforms plastically, thus, compacting the power; the elevated temperatures allow sintering to be performed simultaneously. After sintering the container is removed from the part and additional machining is performed if necessary. The biggest advantage of HIP is that it results in near full density components.

2.3.3 Uniaxial Die Compaction

Uniaxial die compaction is used extensively to produce high part volumes with little material waste and is the dominant method of PM part forming in the automotive parts manufacturing industry. Uniaxial die compaction, in its most basic form, places powder in a die (in the

general shape of the desired part) and pressure is applied via rigid punches. Pressure can either be applied in one direction; single action compaction, or it can be applied from the top and the bottom simultaneously; double action compaction. The stages of single action compaction are shown in Figure 3.

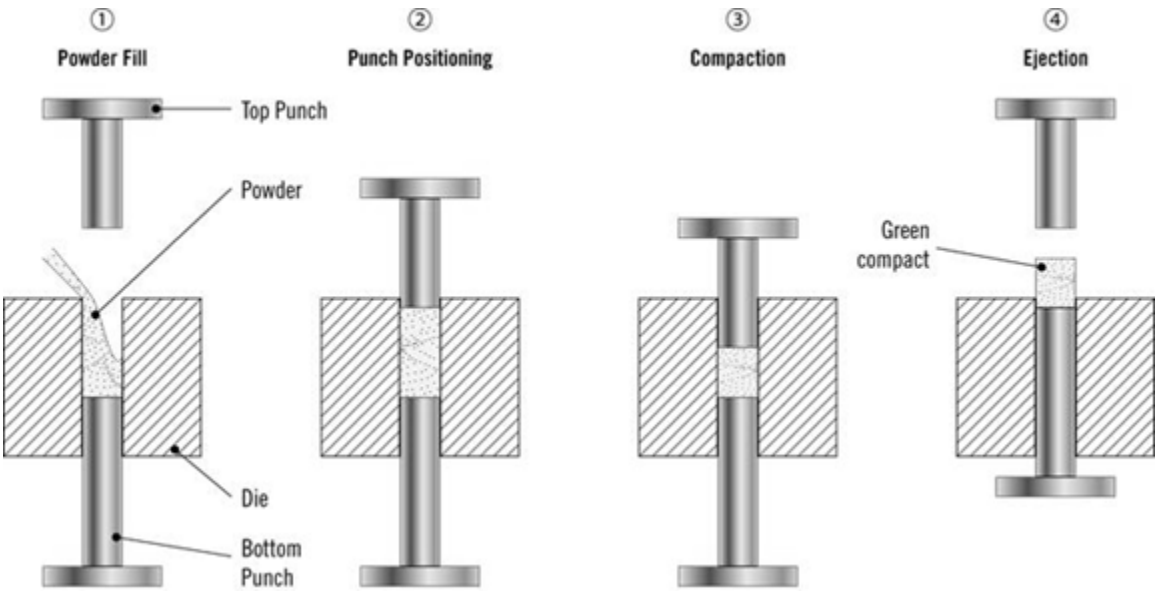

Figure 3: Stages in die compaction. Step 1: Powder is inserted into the die. Step 2: The punches are positioned. Step 3: Powder compaction is performed (either single or double action). Step 4: A green compact is ejected.

An additional method of uniaxial die compaction is the floating die set-up, a schematic of which is shown in Figure 4. The goal of the floating die set up to simulate double action compaction in a laboratory setting without the need for very large and expensive industrial-grade double action presses. The floating die allows the die by to move relative to the top and bottom punches during the compaction process through the use of springs. As pressure is applied to the top punch, the die wall friction causes the die to compress the supporting springs. Even though the lower punch is fixed at the same location as the springs the spring compression allows for movement of the bottom punch towards the middle of the die (German, 2005). The movement of the bottom and top punch towards the center of the die creates a double action compaction effect.

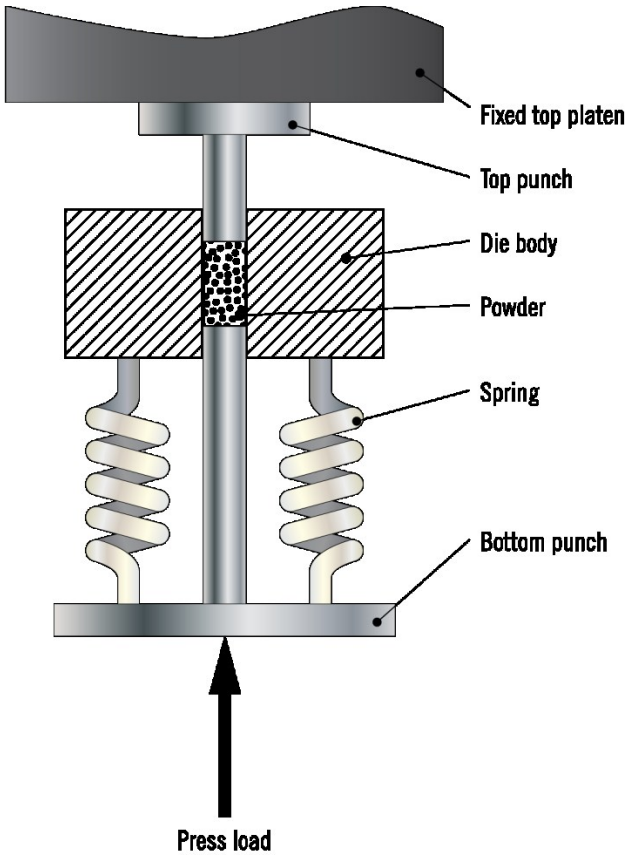

Figure 4: Floating die system illustrating press loading direction, spring supports, die body and powder.

Powder densification during the uniaxial die compaction process can be characterized by four areas: (1) particle rearrangement, (2) localized deformation, (3) homogenous deformation and (4) bulk compression. These stages are depicted on a generalized compaction curve in Figure 5. Firstly, as pressure is applied by the punches, the powder particles rearrange themselves to reduce the volume of empty space without any deformation occurring to the powder; in this rearrangement stage there is the most rapid increase in density. As the pressure application continues, particles begin to deform where they interact; for example two sphere particles at a point contact will begin to have a flattened contact. This stage is referred to as localized deformation. The next stage in compaction is homogeneous deformation where the voids between the particles begin to collapse and the initial particle shape is no longer recognizable, most particles will have a polygonal shape. The final stage of com-

paction is bulk deformation. In this stage of compaction the voids are no longer collapsing and the whole compact is behaving as a solid; there is a very little increase in density.

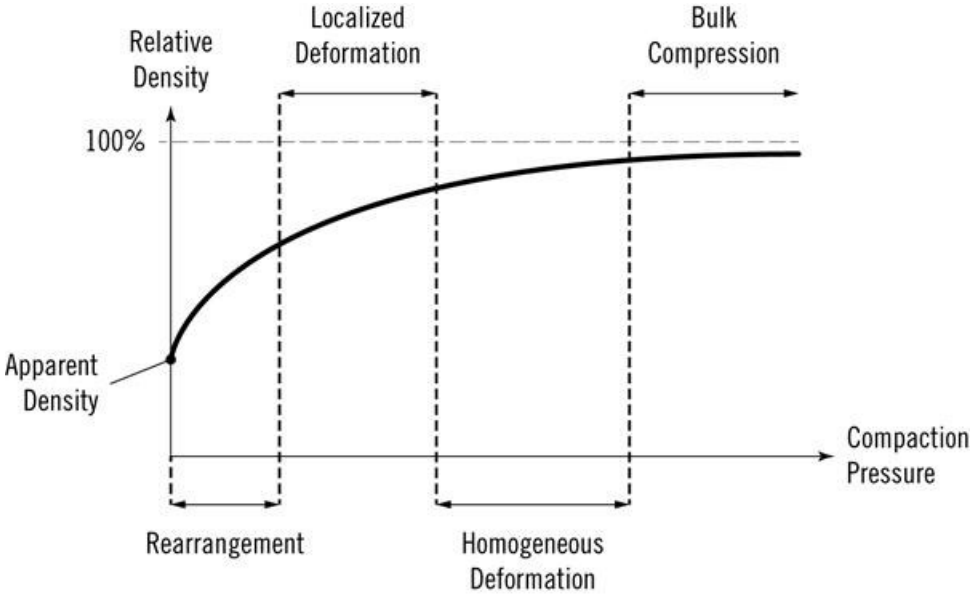

Figure 5: Four stages of densification in uniaxial die compaction: (1) particle rearrangement, (2) localized deformation, (3) homogenous deformation and (4) bulk compression.

One of the most critical drawbacks of uniaxial die compaction is the presence of friction between the die wall and the powder. Die wall friction causes degradation of the applied pressure through the longitudinal axis of the compact, which in turn reduces powder densification. In single action compaction the pressure will be the lowest at the bottom of the compact and this will be the area of lowest density. In double action compaction this same phenomenon occurs; however, the application force is degraded towards the middle of the compact, with the minimum applied pressure occurring in the center; this location is termed the density split. Naturally, as a result of the difference in force application there exists density gradients that follow the degradation of force application. Density gradients are of particular importance because they can cause part failure in areas of low density. Idealized density gradients, or maps, of cylindrical samples for both double action and single action compaction are shown in Figure 6.

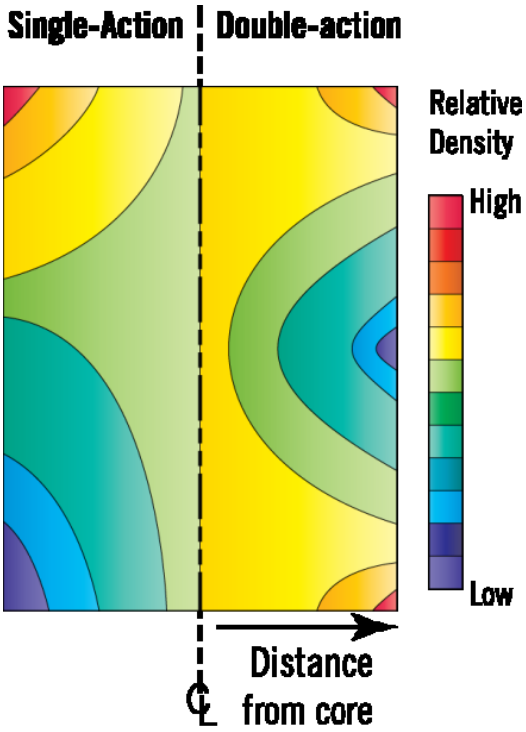

Figure 6: Idealized density gradients for single (left) and double action (right) compaction.

In an effort to counteract density gradients lubrication can be employed. There are two general routes of lubrication application: solid wax mixed into the powder or a liquid sprayed on to the die wall. However, solid wax is generally more popular for high volume application because die wall lubrication has to be applied before prior to powder fill (German, 2005). Typically between 0.7 and 1.5 wt% lubricant is added to the powder before compaction depending on powder material. Not only does the lubrication reduce density gradients but it also helps to reduce wear on tooling and thus extends tool life. Lubrication is expelled prior to sintering by raising the temperature to a sufficiently high temperature.

Other factors that play important roles in the die compaction process are powder size and powder morphology. Powder size is important because it is more difficult to compress smaller particles since smaller particles tend to be harder and strain harden quickly. Conversely, often the powders that press to the highest green densities are large, soft particles. Furthermore, powder shape effects the compaction process because there tends to be an

increased particle friction in smaller and irregularly (generally speaking, non-spherical) shaped powders. However, the green density of powders reaches a maximum at a blend of approximately 70% coarse, 30% fine particles (German. 2005); this is a result of a very high apparent density caused by smaller particles filling voids created by larger particles.

Powder morphology also plays an important role in that each powder shape has distinct compaction characteristics. Particles with a sponge shape are often difficult to compress because it takes a great deal of energy to collapse the internal porosity. Furthermore, irregular particles, while harder to compress, often exhibit excellent green strength properties because of the interlocking characteristics of the irregular shapes. Spherical particles have excellent flow characteristics and low inter-particle friction; however, they exhibit relatively low green strength characteristics. Most often, irregular shaped particles will yield lower green densities than their rounded and spherical counter parts but higher green strengths.

2.4 Sintering Processes

After powder compaction, sintering is employed to induce bonding of the powder particles which enhances mechanical properties. Generally speaking, sintering involves heating the compact to temperatures approaching the melting point of the material, which bonds adjacent particles. This process can occur in two forms: solid state, and liquid phase. Solid state sintering is performed below the melting point of the material and functions by reducing the compact surface energy by way of mass transport mechanisms. Liquid phase sintering is performed at or very near the melting point of the material. During the sintering process a liquid phase is formed which drastically increases the mass transport mechanisms. Aluminum alloys are exclusively sintered using liquid phase sintering as they are often difficult to sinter as a result of an oxide layer that easily forms on the powder surface.

Chapter 3: LITERATURE REVIEW

3.1 The Internal Structure Compact

There are various methods of producing internal structures components; however, there are several benefits of using the PM die compaction method. Mainly, die compaction allows for leveraging the economics of high volume and low cost production capabilities that PM is known for. Additionally, the internal structure compacts offer several unique engineering opportunities that conventional PM compacts cannot fulfill as a result of their solid nature. Internal structure allows for several unique opportunities such as encapsulation of sensors and other internal materials. Fluids contained within the structure can allow the compact to be engineered into fuel pellets, or conversely, internal hollow structures can be used to reduce density and thus increase the specific strength. A potential application of the green internal structure compact is flux filled welding and brazing elements. The internal structure would potentially contain the flux, while the metal matrix serves as the filler material.

Currently, little work has been conducted on die compaction of internal structures. However, several PM technologies have been patented that employ internal structures or functionally graded materials densities. Additionally, there has been a relatively large body of research conducted on hollow sphere structures using PM methods, such as powder products and sintering methods which is discussed in detail in Section 3.2.

Functionally graded compacts allow for engineering of density or material gradients within a compact to allow for directional qualities. Seyferth and Czubarow (1995) developed a method for producing a functionally graded material in which ceramic or metal in powdered form were mixed with a binder and applied to a substrate in layers. The amount of binder in the

applied mixture allowed for controlling of shrinkage during the sintering process. However, as no compaction is applied to the power the degree of densification of the composite would be limited. Belhadjamida *et al.* (2011) produced a functionally graded compact by applying a layer of powder/binder mixture to a green compact. The powder/binder mixture is comprised of different material than the green compact there by imparting different physical and mechanical properties to the exterior of the compact. This green compact with the applied layer is then sintered to bond the exterior layer and sinter the compact. Similar to Belhadjamida *et al.*, Watanabe *et al.* (1981) invented a method of coating green PM compacts with an exterior shell. The exterior shell was applied to a mold using electrolysis, after which the whole composite a green compact is inserted into the formed shell. The shell and the compact are then sintered together. McGee and Mikoda (1975) created a bi-material green compact by placing a divider longitudinally in a die and inserting different powders on either side of the divider. After the material was inserted, the divider was removed, and the powder was compacted using die compaction. The method is a simple economical way to produce a graded material using die compaction; however, it doesn't allow for inserting an internal structure within the compact. Although these processes produce functionally graded compacts, they are different from the internal structure compact in that they generally use a multi-step process, or do not use die compaction.

Roush and Clark (1952) developed a method that employed both powder metallurgy and casting techniques to produce hollow poppet valve heads. First a powder compact is formed in the shape of the internal void desired. This compact is then placed in a casting mold and part is cast around the PM compact. Firstly the PM compact should be on the order of 50-60% relative density. Secondly, suitable compact materials include: copper aluminum, titanium or iron powder. However, the selection of the casting material and the compact material

are co-dependent as the casting material melting temperature must be sufficiently low as not to affect the powder compact during the casting process. After the casting process the cast and internal compact are immersed in acid which dissolves the internal compact and leaves a hollow. The hole left by the PM compact is fitted with a plug which is welded into place.

Levinstein and Butts (1969) developed a method for the production of a hollow metal articles using an internal core (consisting of one of the following metal alloys: aluminum, magnesium, zinc, tin, or cadmium) coated by way of an electro or vapour disposition process with 70-95% on the following powders: iron, nickel, cobalt, copper, silver. Once the core is coated with the metal powder the whole assembly is sintered to a temperature above the core melting point but below the exterior melting point. This allows for the diffusion of the core into the outer shell, thus leaving a hollow interior. This process is illustrated in Figure 7.

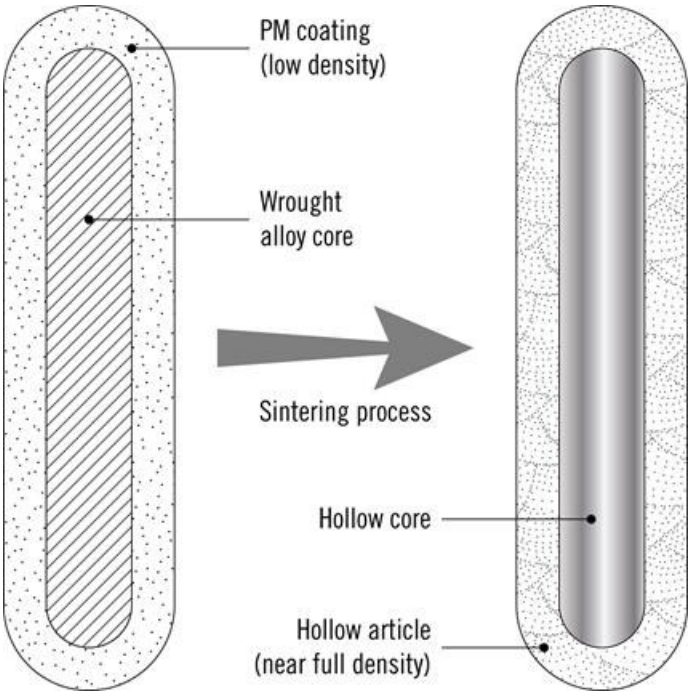

Figure 7: Method of manufacturing a hollow metal article (Adapted from (Levinstein & Butts, 1969)).

Voice and Junfa (2008) created a method of manufacturing hollow fan blades for gas turbines. This method employed filling a hollow container with a metal powder ($Ti_6AL_4V_{60}$) and a metal insert of the same material, coated in a pattern of stop off material, such as yttria. The container is sealed and forged to consolidate the powder. After which, the container is removed from the consolidated powder. A hole is drilled in the tip of the preform and a pipe is connected to the end of the metal insert. The preform and the attached pipe are forged to define the shape of the turbine blade during the forging process; an inert gas is supplied to the turbine blade to inflate the regions where the stop off material was applied to the metal insert to create the internal voids. Lastly, the turbine blade may be finished with necessary grinding or machining operations to attain the proper dimensional tolerances.

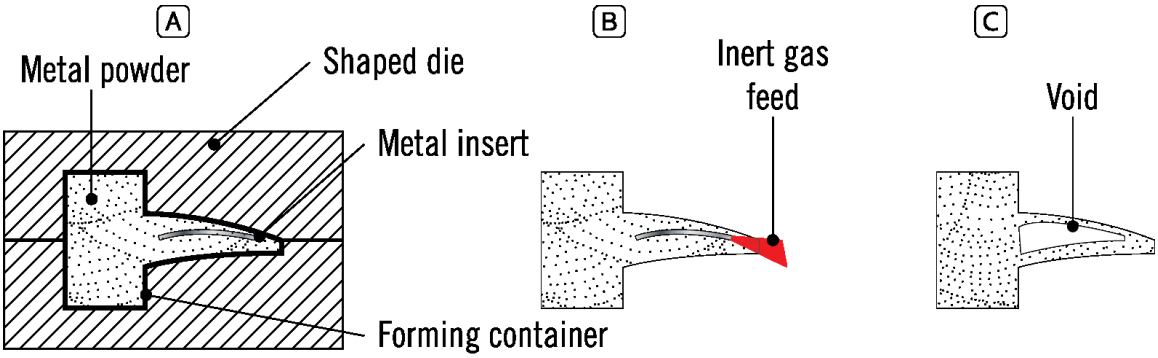

Figure 8: Method of producing hollow fan blades.

Other techniques have been employed to develop hollow parts using PM methods, including; the production of heat exchanger header by Greune (1989) and the production of a hollow ballistic charge by Nguyen (1992). Although, these methods largely focus on producing concave cavities, which are not truly enclosed hollow parts.

3.2 Hollow Sphere Structures

A related type of internal structure compact is one which is developed by agglomerating hollow spheres into a component. These types of components differ from internal structure

compacts in that they do not enclose a single structure within a matrix and as such are better described as foam-like components. However, there is a fairly large body of work in the literature and it is useful here to both provide scope of field as well as serving as a reference point.

Throughout the 20th century many patents were developed around the production of hollow spheres; however, it was not until more recently (1980's and 1990's) that the application of hollow spheres in the production of cellular materials became a focus of the scientific community. Cellular materials can be classified into three types: closed cell metal foams, open cell metal foams and hollow sphere structures. The present discussion will focus on hollow sphere structures, which can be classified into two categories; partial hollow sphere structures and syntactic hollow sphere structures. Conventional metal foams have been excluded from this work as these materials are fundamentally different.

Partial hollow sphere structures consist of hollow spheres bonded together with void space between the spheres, while syntactic hollow sphere structures have a metal matrix surrounding the hollow spheres. Depictions of partial and syntactic hollow sphere structures are shown in Figure 9. Generally, partial hollow sphere structures are fabricated by placing hollow metal spheres in a die and sintering in place to bond the spheres. By contrast, syntactic hollow sphere structures fill the void between the hollow spheres with powdered metal. Upon sintering the powdered metal matrix adds some additional component strength at the expense of increased density. The benefit of hollow sphere structures over conventional metal foams is that they exhibit better compressive strength due to a greater bulk material while still retaining a relatively low density (Sanders & Gibson, 2003). Furthermore, hollow sphere structures are capable of absorbing large amounts of energy at low to moderate stress levels

compared to bulk metals. Greater bulk material allows hollow sphere structures to carry more load then conventional metal foams (Neville & Rabiei, 2008). Currently, hollow sphere structures have a wide base of applications which include: light weight construction, energy absorption applications, explosion protection, sound absorption and medical applications (Andersen, Hungerbach, Stephan, & Studnitzky, 2007).

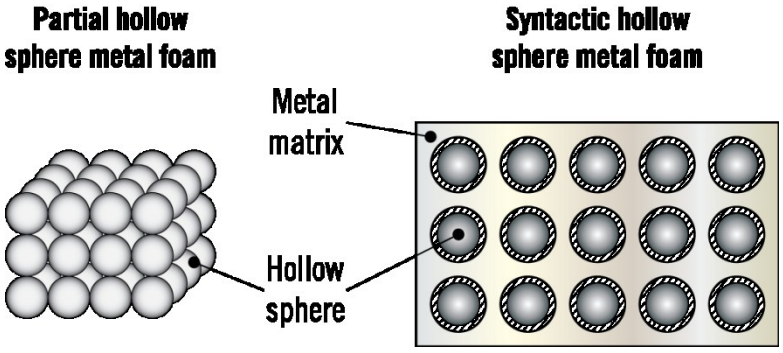

Figure 9: Partial hollow sphere metal foam (left) and syntactic hollow sphere metal foam (right).

3.2.1 Hollow Sphere Production

The production and manufacture of hollow spheres can be classified into three categories:

- Cupping with molds
- PM production
- Chip cutting and assembly of separate parts

Cupping with molds dates to the early 20th century where the first patent awarded to Sphar in 1907. The process, shown in Figure 10, involves pressing a circular blank (Step 1) into a hemispherical shape (Step 2) with a rounded male punch and female die. Next a female punch closes the hemispherical shape to form a hollow sphere (Step 3). This process has been refined and further developed over the years (Gruver, 1917; Isometall, n.d.; Martin, Knight, & Ellis, 1961; Schatz, 1910) but still remains one of the major manufacturing methods of hollow spheres.

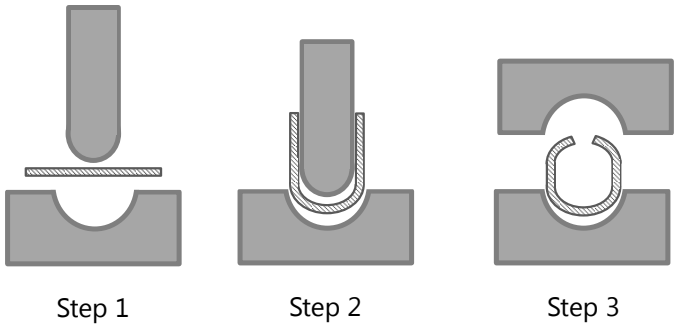

Figure 10: Cupping method for production hollow spheres (Adapted from (Spahr, 1907).

In addition to cupping with molds, the other major production method of hollow spheres is using powder metallurgy processes. The PM production method first starts with a suspension of metal powder, water and binding agent are mixed to create a uniform mixture. Polystyrene spheres are then fluidized in a chamber where the powder suspension is sprayed onto the spheres; after which the spheres are sprayed with a steady air flow to allow the mixture to dry on the foam spheres. If green spheres were desired that process would end here; however, the spheres can be sintered if improved mechanical properties are desired. The final sintering process allows for the pyrolization of the internal polystyrene core, which leaves a hollow sphere. Various researchers have used this method of producing hollow spheres for implementation in hollow sphere structures (Andersen, et al., 2007; Andersen, Waag, Schneider, Stephani, & Kieback, 2000; Augustin & Hungerbach, 2009; Hollomet, n.d.; Ochsner & Augustin, 2007).

Other hollow sphere production techniques involve a range of chip cutting (Rachor & Lotz, 1966), novel forming techniques (Wang & Elleman, 1982) (Geiger, 1946) and assembly of several individual sections (Novak, 1972). These techniques are largely secondary compared to the cupping and PM methods and are not usually used in the hollow sphere structures.

Rachor & Lotz (1966) developed a method of producing hollow graphite sphere using a modified drilling technique. The technique employs a round tipped drill bit and set up that

allows the drill bit to rotate about the x, y, and z axes in relation to the fixed sphere. After the internal sphere is bored out, the hole needed for the drill bit is sealed with a plug.

Novak (1972) created a method of assembling several identical interlocking sections into a hollow sphere. This method was intended to be used for plastic spheres as the sections can be easily molded; however, it is conceivable that this method could be adapted to metals.

Wang & Elleman (1982) created a system to produce gas pressurized hollow spheres for use in nuclear fusion power generation. The method, which shares several similarities to gas atomization, involves a molten material flowing around a pressurized gas nozzle and into a cooling chamber. The two nozzles are nested with the pressurized gas nozzle blowing the molten metal into a hollow sphere; similar to how one would blow a soap bubble.

Geiger (1946) developed a precursor to the current production method of PM produced hollow spheres (described in Section 3.2.2). Refractory hollow spheres were produced by creating a mixture of binder and ceramic material. Combustible pellets several millimeters in diameter are coated in the mixture which is then sintered to remove the internal core and allow the mixture to set.

3.2.2 Partial and Syntactic Hollow Sphere Structures

Currently, hollow metal spheres used for partial and syntactic metal foams are generally produced by PM methods. Partial hollow sphere metal foams are created by bonding hollow metal spheres contained in a form by sintering them in place. These metal foams yield very low densities in the range of 20% of the solid density; however, they show poor compressive strengths due to the lack of bulk material to sustain load (Andersen, et al., 2000; Rabiei & Vendra, 2009). Syntactic hollow sphere metal foams are similar to the above in that the

spaces between the hollow spheres are filled with a metal alloy. After sintering the composite structure shows a higher compressive strength compared to hollow sphere metal foams at the expense of higher relative densities approaching 40% (Neville & Rabiei, 2008).

Andersen *et al.* (2000) developed partial hollow sphere metal foams from PM produced green 316L stainless steel spheres between 0.5 mm and 3 mm diameter. The 316L stainless steel (SS-316L) spheres were created by coating styrofoam spheres with a mixture of water, binder and 316L powder. Spheres were then formed into cylinders with nominal diameters and heights each equaling 24 mm and debinding and sintering were performed in place. The geometrical characteristics of the test samples are shown in Table 1[1].

Table 1: Geometrical characteristics of hollow sphere metal foams. (Adapted from (Andersen, et al., 2000)).

Sample	Hollow Sphere Material	Matrix Material	Sphere Diameter (mm)	Mean Wall Thickness (um)	Sample Diameter (mm)	Sample Height (mm)	Density (g/cm^3)
SS-A-2.5	SS-316L	N/A	2.0-3.0	250	24.7	23.4	1.43
SS-A-0.75	SS-316L	N/A	0.5-1.0	40	24.0	25.8	1.05

It can be seen from Table 1 that samples SS-A-2.5 and SS-A-0.75 both yield relative densities of 20.7% and 15.2%, respectively; however, the nominal compressive yield strength was only 9.0 MPa and 7.4 MPa, respectively; roughly 4% of sintered 316L powder (Andersen, *et al.*, 2000)

Neville & Rabiei (2008) developed syntactic hollow sphere structures with spheres created by Augustin (2009) using a PM processes. Two materials were evaluated; a low carbon steel (LC) and 316L stainless steel; in addition to three sphere diameters: 3.7 mm, 2.0 mm and 1.4

[1]The naming convention used for describing the various samples in this section are as follows: XX-YY-ZZ, where XX is the hollow sphere material, YY is the matrix material and ZZ is the average sphere diameter. For partial hollow sphere structures where no matrix material is used, *A* is used to represent air in the case of regular hollow sphere structures.

mm. Three rectangular samples were created, each with a PM matrix that matched the sphere material. The samples were created by filling a die (51 x 51 x 89 mm) with spheres and after which vibration was applied. Next, the PM matrix was added and the die was vibrated further to achieve a high apparent density (Neville & Rabiei, 2008), and lastly, the samples were sintered in place. Complete sample features are given in Table 2.

Table 2: Sample features for composite hollow sphere metal foams (Adapted from (Neville & Rabiei, 2008)).

Sample	Hollow Sphere Material	Matrix Material	Sphere Diameter (mm)	Mean Wall Thickness (um)	Top face dimension (mm)	Sample Height (mm)	Density (g/cm^3)
LC-PM-3.7	Low carbon steel	PM Low carbon steel	3.7	200	51 x 51	89	3.06
LC-PM-1.4	Low carbon steel	PM Low carbon steel	1.4	50	51 x 51	89	2.55
SS-PM-2.0	SS-316L	PM SS-316L	2.0	100	51 x 51	89	2.95

From the density values presented in Table 2 relative densities for samples LC-PM-3.7, LC-PM-1.4 and SS-PM-2.0 can be calculated as 38.9% and 32.4% and 37.5%. These relative densities are significantly higher than those presented by Andersen *et al.* (2000) for partial hollow sphere structures.

Rabiei and O'Neill (2005) developed a method to produce syntactic hollow sphere structures using a low carbon, and stainless steel hollow spheres (both produced by PM methods) surrounded by aluminum 356 casting alloy (CAl). The production process involves placing the hollow spheres in a casting mold and casing aluminum around the spheres; a schematic of this process is shown in Figure 11. Furthermore, complete geometrical features of the castings are given in Table 3.

Table 3: Sample Features (Adapted from (Rabiei & O'Neill, 2005)).

Sample	Hollow Sphere Material	Matrix Material	Sphere Diameter (mm)	Mean Wall Thickness (um)	Top face dimension (mm)	Sample Height (mm)	Density (g/cm^3)
LC-CAl-3.7	Low carbon steel	Al 356	3.7	200	48 x 35	61	2.41
SS-CAl-3.7	SS	Al 356	3.7	200	36 x 40	53	2.47

The relative densities for samples LC-CAl-3.7 and SS-CAl-3.7 were calculated to be 42% and 43% respectively; this is slightly (5-10% relative density) higher than the relative densities presented by Neville (2008) using a PM alloy rather than a casting as the matrix. Monotonic compression testing was performed on the samples; stress-strain curves from this testing are shown in Figure 12.

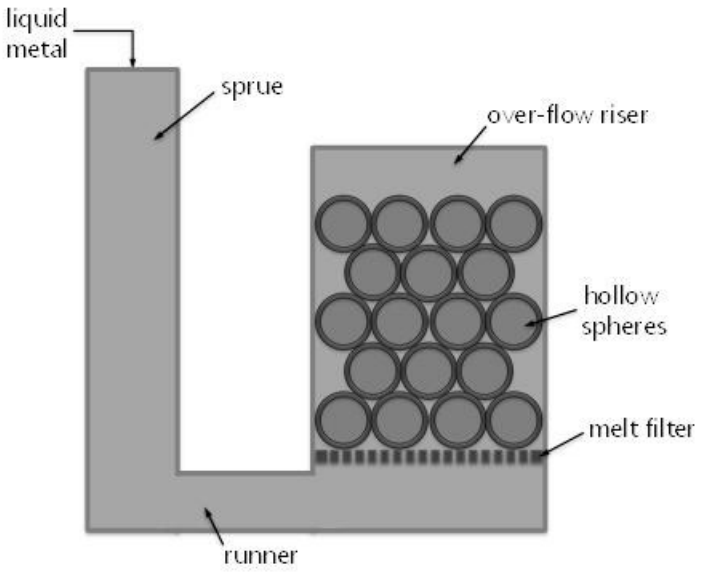

Figure 11: Apparatus for producing metal foams (Adapted from (Rabiei & O'Neill, 2005)).

From Figure 12 it can be seen that all of the various foams show characteristic stress-strain behavior of metal foams. All seven samples showed an initial region of elastic deformation where reversible sphere wall bending occurs (~ 0-1% strain). After which, an extended plateau of relatively constant stress occurs. This region is characterized by plastic deformation in the sphere walls (between approximately one to 50% strain) The last region of the curve

shows a rapid increase in stress caused by the nearly complete densification of the samples and thus behavior similar to a solid metal (Hall, Guden, & Yu, 2000). Two samples; LC-PM-3.7 and SS-CAl-3.7S; showed strain softening (decrease of stress with an increase of strain (Zhan-you, Xian-rong, & Xian-nan, 2007)) at approximately 18 and 10% strain, respectively. Additionally, the SS-CAL-3.7 sample appears to be able handle the largest loads before densification; however, densification occurs at roughly 40% strain compared to 55-65% strain of the other samples. Furthermore, the plateau region of the SS-CAL-3.7 sample is quite steep with linearly increasing stress. It is clear from the figure below that the syntactic structures (SS-PM-2.0, SS-CAL-3.7, LC-PM-3.7, LC-PM-1.4 and LC-CAL-3.7) outperform partial structures (SS-A-0.75 and SS-A-2.5) in terms of sustained load in the plateau region of the stress-strain curve. This is attributed a greater amount of bulk material available to sustain compression load. However, regular hollow sphere structures were able achieve greater strains (upwards of 70%) compared to composite hollow sphere structures before densification. In addition to the stress-strain curve presented in Figure 12, the energy absorption characteristics of the various hollow sphere structures are given in Table 4.

Interestingly, from Table 4 it can be seen that hollow sphere samples SS-A-2.5 and SS-A-0.75 have comparable energy absorption (kJ/kg) characteristics to LC-PM-3.7; however, the relative density is approximately 20 to 25% less. Furthermore, SS-PM-2.0 has significantly higher energy absorption per kilogram of material and plateau stress per density compared to the other syntactic hollow sphere structures while maintaining a comparable relative density. Comparisons can be made between samples LC-PM-3.7 and LC-PM-1.4 to illustrate the tradeoffs between internal sphere sizes. Sample LC-PM-1.4 shows better mechanical properties in terms of plateau stress and energy absorption while maintaining a lower density than its LC-PM-3.7 counterpart.

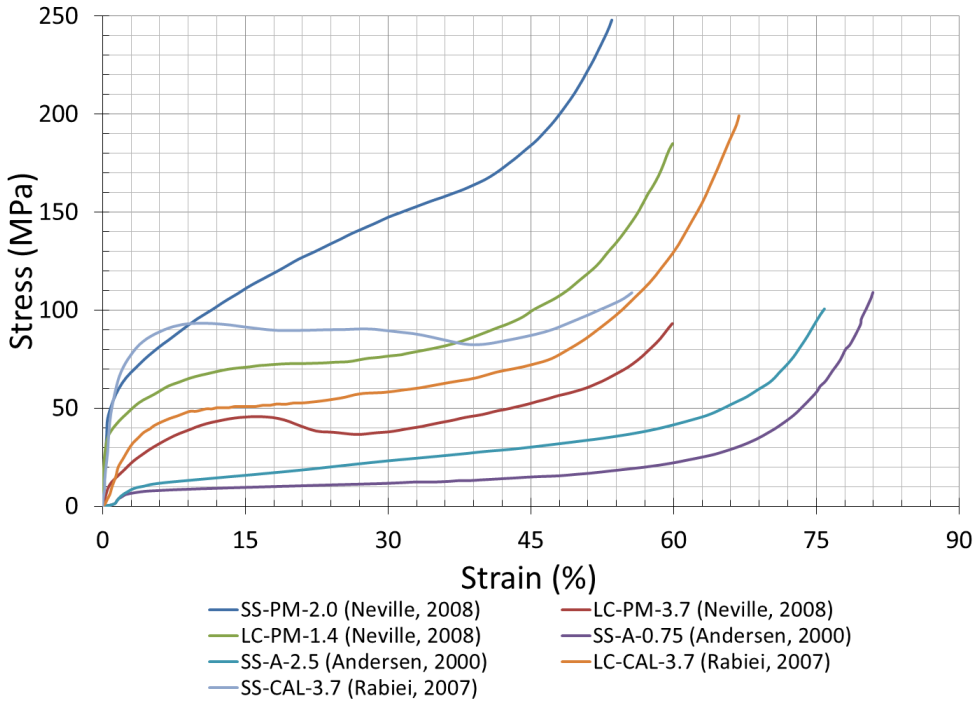

Figure 12: Comparison of stress-strain curves for metal foams.

Table 4: Mechanical properties of various metal foams.

Reference	Sample	Plateau Stress (MPa)[2]	Plateau Stress (MPa/(g/cm^3)	Energy Absorption (MJ/m^3) @ 50% Strain	Energy Absorption (kJ/kg) @ 50% Strain	Measured Density (g/cm^3)	Relative Density (%)
Andersen (2000)	SS-A-2.5	19.07	13.34	10.12	7.08	1.43	20.7
Andersen (2000)	SS-A-0.75	11.03	10.51	5.43	5.17	1.05	15.2
Neville (2008)	LC-PM-3.7	41.11	13.44	20.43	6.68	3.06	38.9
Neville (2008)	LC-PM-1.4	72.40	28.39	37.91	14.87	2.55	32.4
Neville (2008)	SS-PM-2.0	123.0	41.70	67.71	23.0	2.95	37.5
Rabiei (2007)	LC-CAL-3.7	53.0	22.0	27.57	11.44	2.41	42.3
Rabiei (2007)	SS-CAL-3.7	90.66	36.70	43.32	17.54	2.47	43.0

[2] The plateau stress was calculated by acquiring the mean stress between 10 and 30% strain. Similar methods have been proposed by Hall (2000) and Ruan (2002) for calculating the plateau stress.

Conversely, partial hollow sphere structures with larger spheres exhibit better mechanical properties. As stated before, it is theorized that the matrix material allows for more bulk material to sustain load. If one compares samples SS-PM-2.0 and SS-A-2.5 it is clear that the former sample outperforms the latter in all aspects aside from relative density while the sphere materials are identical and sphere diameters are in the same size range, and the only major difference being the internal matrix material.

In addition to experimental testing, various finite element models have been created to study the mechanics of hollow sphere structures including Oliveria *et al.* (2009). Their work studied the mechanical behavior of partial and syntactic hollow sphere structures using PM hollow spheres. The model was able to show deformation characteristics of hollow spheres and hollow sphere structures, however, the work was mainly developmental and focused on model validation rather than actual mechanical performance of different structure designs. Vasenjak *et al.* (2008) studied the behavior of syntactic and partial hollow sphere structures under dynamic loading; specifically primitive cubic, body centered cubic (BCC), and face centered cubic (FCC) arrangements. The work showed that primitive cubic structures were able to sustain higher loads than BCC and FCC orientations for both partial and syntactic structures, in addition to a large stain rate dependence on compressive stress-strain characteristics.

3.3 Densitometry Methods

There are many density analysis techniques that are currently being used in various areas of PM research. In this section, an overview of selected density analysis techniques will be presented with a special focus on the benefits and drawbacks of each method.

3.3.1 Archimedes Method

Perhaps the most basic method to measure density is Archimedes method. First, the mass of the part is weighed, and next the part is submerged in water. Knowing the resulting change in total volume; the part volume can be determined and thus the part density can be determined. Density maps can be created using this method by sectioning the part into smaller masses; however, the resolution is limited by the size that can be cut from the initial part. Also, one of the biggest issues with this method is possibility of water infiltrating the part and thus giving an improper part volume. Furthermore, this method is rather crude (for density maps) as a result of part mass being lost to cutting and thus highly accurate results cannot be expected. Furthermore, for low pressure green compacts sectioning the part into small samples is often difficult given the low strength of the compact.

A refined Archimedes method involves measuring the mass of the part in air and water. Knowing the density of water, the density of the part can be determined. This method is more accurate because one is only limited by the accuracy of the thermometer (needed for determining water density) and the scale. However, issues still exist with water infiltration and thus, this method is still largely limited to complete parts.

3.3.2 Gamma Ray Detection

Gamma radiation is an electromagnetic radiation similar to x-rays that are generated by the decay of radio nuclides. The principle of gamma radiation detection is the radiation penetrates the part in question and some of the radiation is absorbed within the particle. The absorbed radiation causes a decrease in the incident radiation intensity. Using the material and radiation source properties, the decrease in incident radiation intensity can be correlated to the part density.

The gamma ray density measurement system is shown in Figure 13. A small stream of gamma radiation is allowed to emit from a radiation source that is enclosed in a container. The radiation is exposed to the part which then passes through and is filtered using an aperture. Finally, the resultant radiation flow is measured using a detector and is correlated to the part density in the specific location.

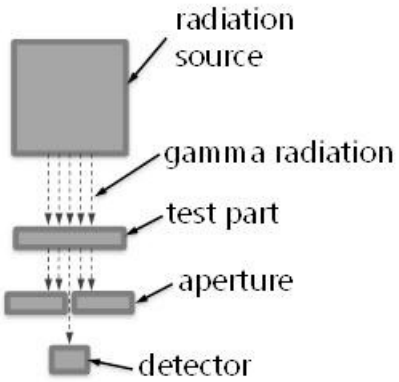

Figure 13: Gamma ray detection density equipment (Adapted from (Schlieper, 2010))

The gamma ray method is able to measure regional densities (test points) (Schlieper, 2000) however, there is no way to measure multiple densities through the width of the part (without sectioning), and it is not possible to measure the density along a sloping part feature such as a chamfer (Schlieper, 2010). The most significant drawback of this method is that different intensity radiation sources are needed for different materials (Haggblad & Oldenburg, 1994). Thus, the issues arise with this method with regards to safety and control issues associated with the radiation source (Schlieper, 2000). Nevertheless, Stepanenko *et al.* (1984) were able to measure densities across the face of a copper compact to within an error of 3%.

3.3.3 X-Ray Computed Tomography

X-Ray computed tomography (CT) is a non-destructive method of imaging internal sections through the use of an x-ray. This imaging technique can be calibrated to measure density distributions across internal planes through a compact. X-Ray CT is performed by placing the

part in question on a turn table and rotating while it is irradiated with x-rays. A detector is then used to measure the intensity of the x-rays that pass through the compact. This equipment can be visualized in Figure 14. From the detector, mathematical relations can then be used correlate the intensity of the x-ray to the density of the compact (Sinka, Burth, Tweed, & Cunningham, 2004). X-Ray CT is widely used in medical fields for internal body images and industrial fields for failure analysis and flaw detection (Li, Nam, & Lannutti, 2002).

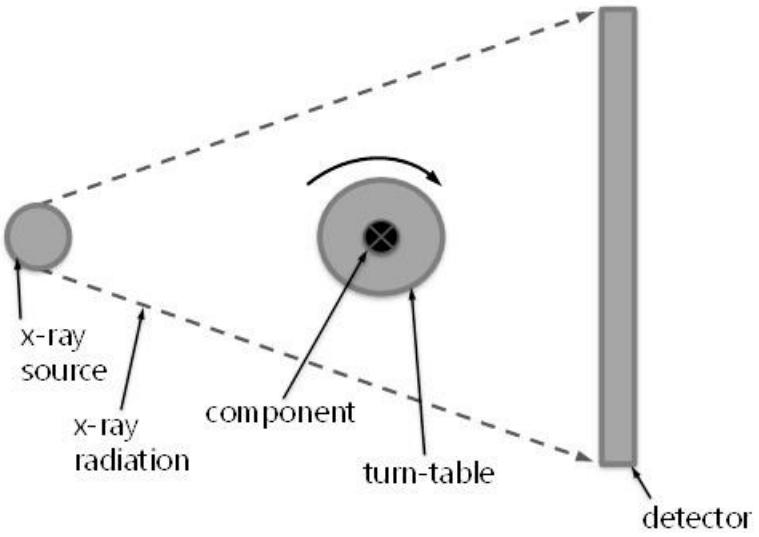

Figure 14: X-Ray computed tomography equipment set-up (Adapted from (Sinka, et al., 2004)).

X-Ray CT is a valuable tool because density analysis can be performed in a non-destructive manner; that is, one can analyze all aspects of a single component which allows for part to part testing. With destructive techniques numerous areas on one part cannot be tested at the same time and thus it maybe come difficult to study correlated effects within a single compact. Furthermore, X-ray CT allows for imaging of an entire cross section with a fairly high resolution of 0.2 mm, however, the depth resolution is approximately 2 mm (Li, *et al.*, 2002). X-Ray CT is a fast method of analyzing density distribution approximately taking 20 minutes per scan; however, the major drawback is that it is an expensive technology. Other issues

associated with X-Ray CT is that some materials, such as lead and magnetic powders, cannot be measured because some materials (such as lead) are impermeable to X-rays.

3.3.4 Double Correlation Technique

Weber and Brown (1989) developed a double correlation technique that first correlates green powder compact density to an identical sintered compact; this is then correlated to the Rockwell hardness of the sintered part. This is similar to Archimedes method in that it can create crude density contours; and it is possible for large inaccuracies to exist (Kandeil *et al.* 1977). Although, it is possible to measure large density gradients across a compact and thus the density difference between top and bottom punches, for example, can be easily measured. Kandeil *et al.* (1977) developed a double correlation technique which was slightly modified from Weber and Brown (1989). First, a compaction curve was created, next, it was postulated that a linear relationship exists between hardness and compaction pressure because such a relationship exists between material yield and hardness. The basis for this hypothesis was rooted in the fact that the pressure to which the compact was formed corresponds to the yield strength of said compact. Finally, using the compaction curve and the relationship between hardness and compaction pressure, density and hardness were correlated. This method was used to create a density map for a die compaction sample which yielded promising results for single action compaction similar to those shown by German (2005). However, the results shown were an average of several individual density maps and still resulted in an error of approximately 5%.

3.3.5 Optical Densitometry

Optical densitometry is a density analysis method that is currently gaining popularity as a means to analyze density gradients within a compact (Ma, Zahrah, & Fields, 2004; Mccabe,

Godby, & Trasorras, 1994; Molinari et al., 2011; Sanderow & Murphy, 2000). Generally, optical densitometry involves polishing the surface of the compact and investigating the surface using a microscope and image analysis software. The density is calculated based on the ratio of dark pixels (pores) to light pixels (bulk material). This technique has been used in several different ways, such as analyzing surface densification (Molinari, et al., 2011), validating FEM models (Ma, et al., 2004)and producing density contours of compacted samples (Beck, Selig, Doman, & Plucknett, 2011).

Molinari *et al.* (2011) utilized optical densitometry to measure surface densification layer of shot peened Cr-Mo steel samples. Optical micrographs of the desired locations were obtained and analyzed. Firstly, the background illumination of the micrograph was estimated, this was subtracted from the original micrograph. The resulting gray scale image was separated into a binary form (white pores and black background). The binary image was analyzed in pixel columns to represent porosity as a function of depth. This method was able to accurately produce densification as a function of depth; however it was not intended to produce density gradients across a compact surface.

Ma *et al.* (2004) employed optical densitometry to validate a gear finite element (FE) model. The face of a compact was polished and micrographs were obtained at eight locations across the compact. Each image was analyzed and the percent relative density was calculated. The obtained data were then compared to density values obtained from an FE simulation as a means to validate the model. Similar to Molinari *et al.* (2011), the method employed was not used to produce density gradients plots.

McCabe *et al.* (1994) investigated the effectiveness of optical densitometry to produce density maps of steel compacts to validate finite element simulations. Steel powder was pressed to a

height of 3.175 mm and 25.4 mm in diameter in a floating die at 260, 440, and 615 MPa. The samples were then lightly sintered, sectioned through the mid plane, mounted in epoxy, and polished. Images with a spatial resolution of 0.762 by 0.635 mm at a magnification of 100X were acquired in a grid format across the face of the compact and analyzed for percentage of porosity or darkness in the image. Five samples were analyzed for each compaction pressure the corresponding data points of the five density maps were then averaged to produce a final map for each pressure. Averaging the five density maps produced a final map that showed fewer anomalies and also more closely match the bulk density measurements. The optical densitometry data, compared to the bulk density measurements (Archimedes' method) are given in Table 5. Both methods of density measurement showed comparable results, however slight differences between methods were recorded.

Table 5: Density Measurements (Adapted from (Mccabe, et al., 1994)).

Compaction Pressure (MPa)	Density (g/cm^3, bulk, Archimedes' method)	Relative Density (bulk, Archimedes' method)	Relative Density (averaged, optical method)
260	5.9	75%	75%
440	6.5	83%	81%
615	6.9	87%	88%

Sanderow and Murphy (2000) conducted an inter-laboratory study to determine the uncertainty of optical densitometry. The study employed ten labs that used optical densitometry to measure densities at two specified locations on transverse rupture strength bars that were compacted at one location. Two powders were employed: SS-316L and FC-0208. The study concluded that optical densitometry had a reproducibility of 7.5% and a repeatability of 2.7%. The repeatability is comparable to bulk density measurements using (ASTM, 2003), however, the reproducibility is nearly double. It was shown that more variation occurred in the in SS-316L sample, this was attributed the softer material being more difficult to polish consistently. Furthermore, threshold analysis was performed at 5 point intervals on FC-0208

at various magnifications to determine the effect of changing the threshold value as well as magnification. Images were taken in a 5x5 grid (and the data was averaged) pattern at 50, 100 and 200 times magnification and the threshold was varied from 115 to 135. The results of the threshold study are presented in Figure 15. It can be seen that the relative density measurement varies the most at 50x magnification, in addition to lower sensitivity at 200X magnification, suggesting that increasing the resolution of the system has a greater effect on the results than the threshold selected (Sanderow & Murphy, 2000). In addition to threshold analysis, field to field variation tests were performed by acquiring images in a continuous strip along the longitudinal direction at 100 and 200X magnification. The results showed that large variation (>8%) were present between neighbouring fields at 200X, this was greatly reduced to 3% at 100X.

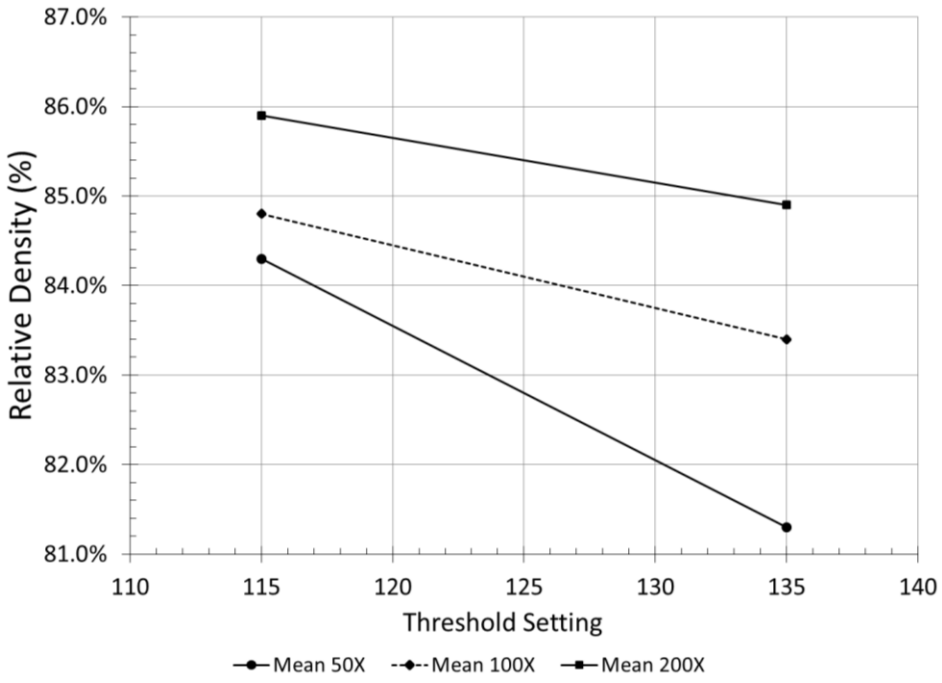

Figure 15: Relative density versus threshold (Adapted from (Sanderow & Murphy, 2000)).

3.4 Die instrumentation

Die instrumentation is critical in assessing the compaction process. Various researchers have employed instrumentation to measure friction, die stress, compaction pressure, and *in situ* density. The instrumentation data are then able to help address and solve problems in the compaction process. Additionally, the data can be used to develop constitiuve data for implementation into finite element models.

Guyoncourt *et al.* (2001) employed an instrumented die set up to measure friction stress, friction coefficient, density, and radial stress in situ for uniaxial single action compaction. The setup, shown in Figure 16, employs load cells to measure top and bottom punch displacements and radial stress sensor embedded in the die and finally a linear variable displacement transducer (LVDT) to measure top punch displacement. In situ density measurements were acquired by employing the LVDT to measure the compact height during compaction, knowing the initial fill height and the die dimensions, the density was calculated. It was stated that margin of error was 5%. This setup was mainly used to acquire constitutive data and friction coefficient measurements. The results were promising; the set up was able to distinguish between different batches of the same powder for friction measurements.

Instrumented die set-ups have been adapted to measure powder/die interface friction. The friction coefficient can be deduced from top and bottom punch stresses, as well as, radial stresses measured in an instrumented die. The friction is given by:

$$\mu = \frac{D}{4kh}(ln\sigma_{zt} - ln\sigma_{zb}) \tag{1}$$

$$k = \frac{\sigma_r}{\sigma_z} \tag{2}$$

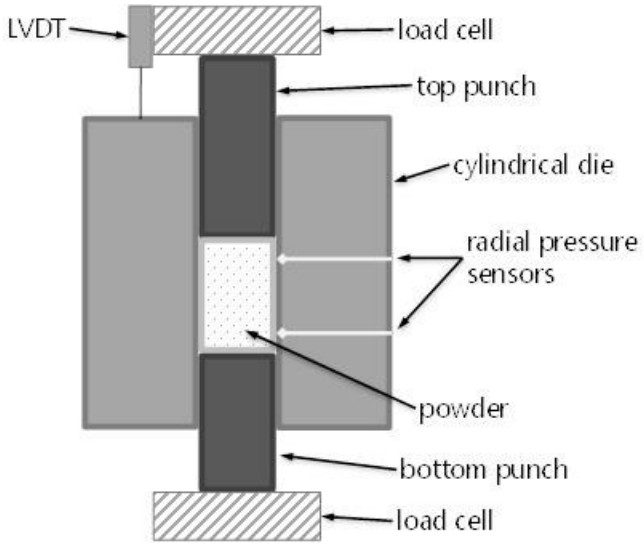

Figure 16: Guyoncourt instrumented die set up.

The full derivation of this equation is given by Brein *et al.* (2010): where D is the compact diameter, σ_{zt} is the axial stress at the top punch, σ_{zb} is the axial stress at the bottom punch, k is the ratio of average compaction pressure (σ_z) to radial stress (σ_r) and h is the length of the compact. As it can be difficult to measure radial stress within the die, an alternative method of measuring friction has been developed using a shear plate technique (Brewin, Coube, Doremus, & Tweed, 2010). The shear plate technique involves compacting a sample in a die and applying pressure as a plate is moved across the powder compact. The force required to move the plate and thus, the friction coefficient can be deduced using equation 3.

$$\mu = \frac{F_S}{F_N} \tag{3}$$

Where F_S is the force required to move the shear plate and F_N is the normal force applied to the compact. The benefit of this method, of the instrumented die method is different die conditions can be easily measured by changing the shear plate.

Chapter 4: EXPERIMENTAL METHODS

This section outlines the materials and methodology for the production of internal structure compacts. Additionally, the experimental methods for density measurements (both bulk density and density gradients) and compressive green strength (CGS) testing are detailed.

4.1 Materials

The powder used as the matrix material of the internal structure compact is ECKA Granules Alumix 321, which is analogous to Al6061. The material composition of Alumix 321 is given in Table 6. This material was selected as base matrix because it is a well understood and documented powder (Selig, 2012; Selig & Doman, 2011a, 2011b). The cavity shell material was a sphere made of Al3003, the material properties are shown in Table 6. Al3003 was selected as the cavity shell material due to its machinability and ductile properties.

Table 6: Nominal chemistry of Alumix 321 and Al3003 (Granules, 2012; MatWeb, 2012).

Alloy	Mg %	Mn %	Si %	Cu %	Fe %	Zn %	Microwax C (lubricant)	Al %
Alumix 321	1.0	N/A	0.5	0.2	N/A	N/A	1.5	remainder
Al3003	N/A	1.0-1.5	0.6	0.05-0.2	0.7	0.1	N/A	remainder

Stearic acid ($C_3H_5(C_{18}H_{35}O_2)_3$) was selected as the cavity fill because it is readily available at an inexpensive cost and it allows for processing many spheres in a batch process; furthermore, it is similar to microwax C lubricant contained in the Alumix 321 powder, in that they are both fatty acid based waxes. The material composition is given in Table 7.

Table 7: Material properties of Stearic Acid (O'Neil, 2006).

Material	C %	H %	0 %	Melting Point (°C)	Density (g/cc)
Stearin	76.8	12.4	10.8	55	0.862

4.2 Internal Structure Production

The internal structure employed for this work was a commercially available 6.35 mm diameter Al3003 hollow sphere. The complete internal structure was produced by drilling a 2 mm hole through the center of the center of the Al3003 cavity shell. After which, stearic acid was heated to approximately 70ºC and the cavity shells were immersed in the liquid stearic acid. The stearic acid was then removed from the heat source and allowed to cool to room temperature. The cavity shells were then removed from the solid stearic acid and any excess that remained on the external surface of the cavity shell was removed.

4.3 Die Compaction

Single action die compaction was carried out in a 12-ton Model C Carver® press. The single action set up employed a stationary lower punch located at the die/platen interface and a moving top punch placed in the top of the custom made die. An Omega LC8300-500-100K load cell was employed to measure the maximum top punch force and a Celesco PT101 draw wire transducer was used to measure top punch displacement.

The method used to produce these components has three general steps described below:

Step 1

- Weigh out the desired mass of Alumix 321 powder.
- Transfer the powder to the die cavity.
- Tap the die to achieve a flat powder surface.
- Insert the internal structure.

Step 2

- Weight out the desired mass of Alumix 321 powder.
- Transfer the powder to the die cavity.
- Tap the die to achieve a flat powder surface.
- Insert the upper punch and load cell.

Step 3

- Measure to the top of the upper punch using a height gage.
- Press the sample to the desired compaction pressure measured from the load cell.
- Eject the compact.

Figure 17 shows a schematic of the steps described above. On the left of the figure, the powder is inserted into the die, after which, the internal structure is inserted and the final powder fill is completed. Figure 17 also shows where the hole (that allows the stearic acid to fill the structure) is located during compaction. Additionally, conventional samples were compacted at 100, 200, 300 and 400 MPa; the power mass of the conventional samples was selected so that the final compacted heights would be nearly equal to the internal structure samples. The power mass for the conventional and internal structure samples is given in Table 8; masses were weighed to ±0.002 g of the nominal mass using a Sartorius ELT103 scale. For the internal structure samples the powder was inserted in two parts, thus 3.15 g was weighed at a time. Five samples were compacted at each pressure to allow for repeatability, as well as measurement of the bulk density, green strength and optical densitometry.

Table 8: Powder mass for conventional and internal structure samples.

Sample Type	Mass ±0.002 (g)
Conventional Compacts	6.650
Internal Structure Compacts	6.300 (3.150/3.150)

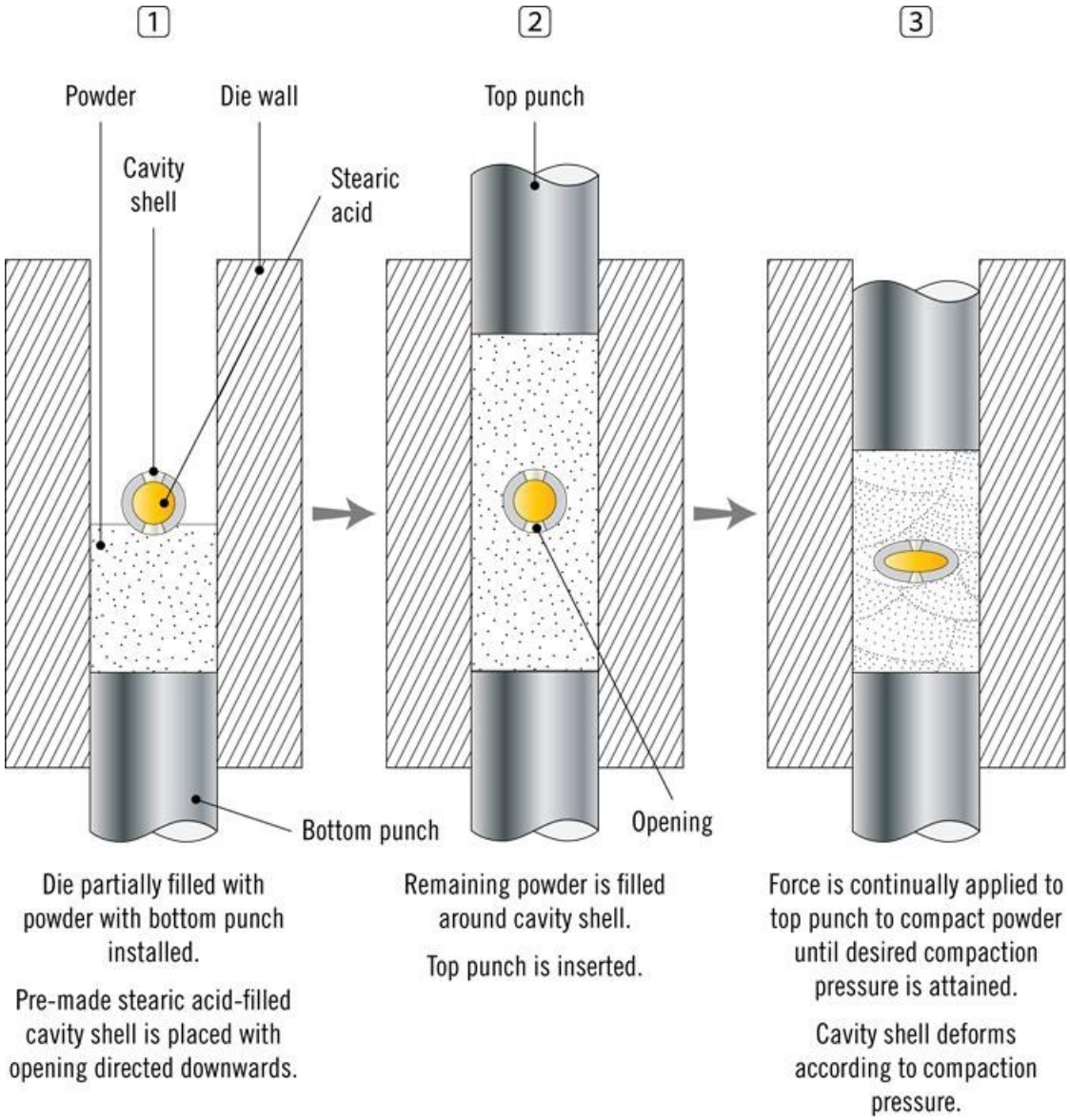

Figure 17: Die compaction stages of the internal structure compact. On the left initial powder and structure insertion, followed by final powder fill and die compaction.

4.4 Density Measurements

Bulk density measurements where completed by measuring the height and diameter of each sample with a Mitutoyo 293-831 micrometer accurate to 0.001 mm. The samples were weighed to the nearest 0.001 g using a Sartorius ELT103 scale. From this data the density of the specimen can be determined as:

$$\rho_G = 1273.24 \frac{m_g}{d^2 h} \quad (4)$$

Where ρ_G = the sample density in g/cm^3, m_g = the sample mass in g, d = the diameter of the sample, and h = the height of the sample in mm.

4.5 Optical Densitometry Measurements

Density gradients were measured using an optical densitometry method. The process first involves mounting complete the sample in epoxy (Buehler Epo-Thin epoxy). After the epoxy has cured (approximately 24 hours) the sample is sectioned along the mid plane using 240 grit silicon carbide paper and water. After sectioning, the sample was polished using a Behuler 60-1990 automatic polisher following the steps outlined in Table 9.

Table 9: Polishing procedure for green aluminum compacts.

Surface	Abrasive Size	Load (lbs)	Base Speed (RPM)/Direction	Time (min)
Waterproof paper	240 grit SiC	3	260 – complementary	Until plane
Ultra-Pol	9um Diamond Suspension	3	150 – complementary	6
Trident	3um Diamond Suspension	3	150 – complementary	4
Trident	1um Diamond Paste (applied with extender)	2	150 – contra	3
Microcloth	0.05um Colloidal Sillica	2	150 – contra	3

Once the polishing procedure was completed, the sample was examined using an Olympus BX51 optical microscope with a 5X objective and a QImaging three megapixel camera; images were captured using ImagePro software by Media Cybernetics. Eight bit grey scale images with a spatial resolution 1.78 mm by 2.37 mm and a 1200 x 1600 pixel resolution were captured in a grid pattern on half of the compact (along the compaction axis; shown in Fig-

ure 18). An example of a captured image is shown in Figure 19. The procedure started in the bottom right location and moved down the compact after each image was acquired. Once end of the compact was reached the stage was reset to the starting position and the next row (inwards towards the compact core) was analyzed. Half of the compact surface was analyzed as the cylindrical compact will show axi-symmetric results.

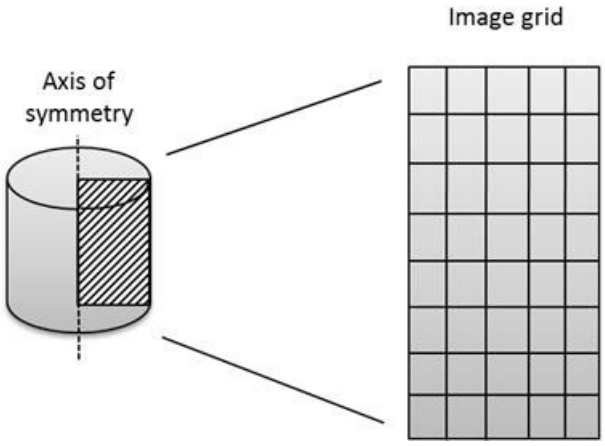

Figure 18: Schematic of compact and approximate grid of images acquired.

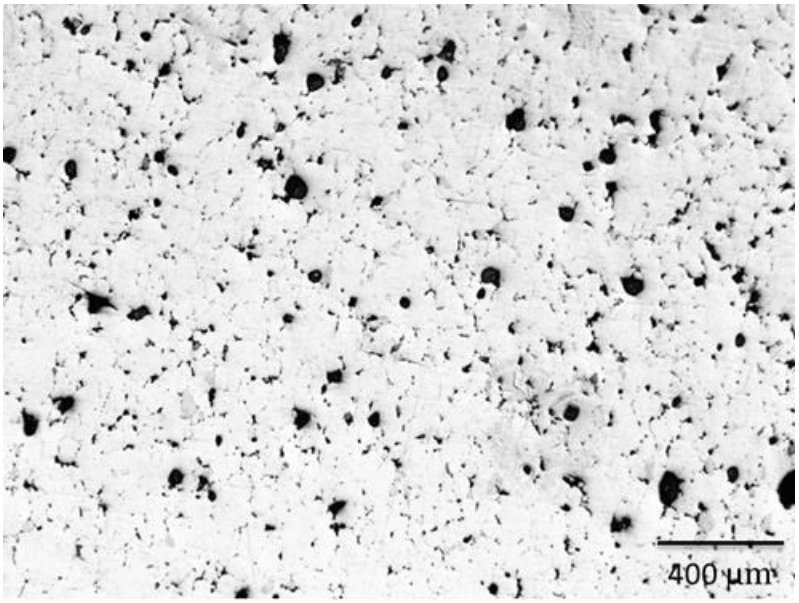

Figure 19: Micrograph taken of polished Alumix 321 sample at 50x magnification and 300 MPa compaction pressure.

The images were analyzed for the relative density by looking at the relative amount of black (which corresponds to pores) compared to the rest of the image. Thus, the relative density, compared to solid aluminum, is described by:

$$Relative\ density\ (\%) = 100\ \% - \%\ black\ (6) \quad (6)$$

Images were processed for the relative density using National Instruments Vision Assistant. Once the image processing was complete for a given sample the resulting data was imported into MATLAB and a density contour map.

As eight bit grey scale images were captured and analyzed a desirable threshold had to be selected by the user. The eight bit images ranged from greyscale value of 0, which is pure black, to 255, which is pure white. The threshold analysis value is defined as the brightest shade of grey that is counted towards the percentage black in the image. As such, as the threshold increases, more shades of grey are counted, and thus, a lower relative density value would be calculated. This phenomenon is shown in Figure 20, where the image on the left is analyzed with a threshold of 75 and the one on the right is analyzed with a threshold of 150 (Selig, 2012). The relative density of the image on the left image is 86.9% (threshold of 75) while the image on the right has a relative density of 79.6% (threshold of 150). As the images can be more or less sensitive to the threshold value depending on the amount of porosity, and it can be difficult to accurately decipher where a pore stops and the compact surface starts, the threshold value was selected to match the bulk density (calculated in Section 4.4) to the average relative density of all of the analyzed images. (Beck, et al., 2011).

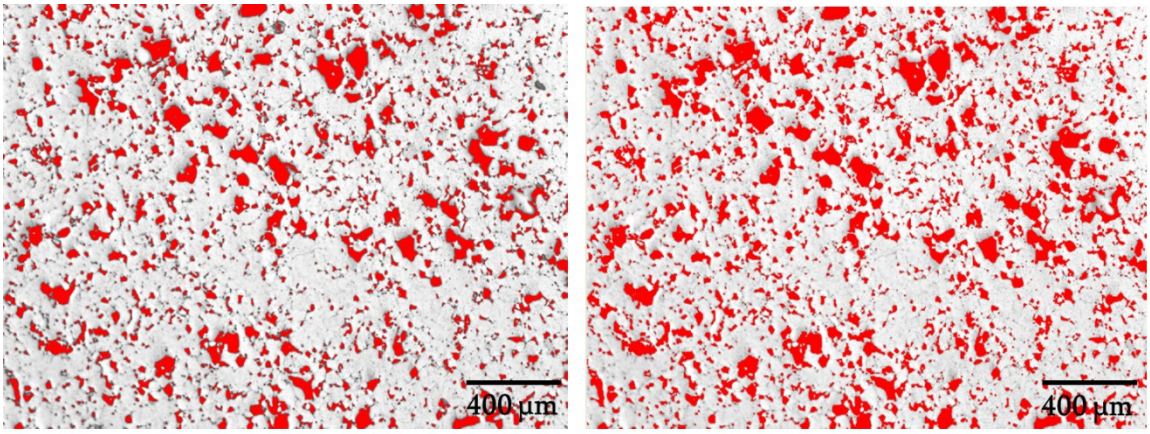

Figure 20: Effect of changing threshold value (from 75 to 150) on compacted Alumix 321 sample. Data analyzed with National Instruments Visions Assistant (Selig, 2012).

4.6 Compressive Green Strength Testing

Compressive green strength (CGS) testing was completed in a Carver® Model C hydraulic press. The testing was completed by placing the compact in question between two flat platens lubricated with a solid stearate. A load cell connected to a National Instruments portable data acquisition system was placed above the top platen to measure the failure load. For the CGS testing the engineering stress was considered; the testing regimen involved loading the compact with the hydraulic press until an observed failure occurred. The CGS of the tested compacts was defined as the ultimate compressive strength recorded before the compact failed by fracture.

Chapter 5: RESULTS

5.1 Preliminary Results

During the preliminary developments of the internal structure compacts various internal structure sizes and fill types were investigated to determine qualitatively what happens during the compaction process. Several cavity shell diameters (6.35, 9.53 and 12.5 mm) with stearic acid fill were investigated to determine effect of size. Generally, 9.53 and 12.5 mm diameters resulted in cracking upon ejection because the powder matrix did not have sufficient strength to withstand the radial stresses around the diameter of the internal structure. Additionally, several fill types were investigated including a stiff epoxy and soft polyurethane foam. The soft polyurethane foam did not have sufficient strength to maintain the internal structure during compaction at 100 MPa, and thus; resulted in complete collapse of the internal structure. A cross section of an internal structure with polyurethane foam at 100 MPa is shown in Figure 21 A which shows a collapse of the cavity shell since the foam was too soft. Conversely, the epoxy fill was stiff enough to maintain the internal structure geometry, however; the compact, which is shown in Figure 21 B, cracked upon ejection.

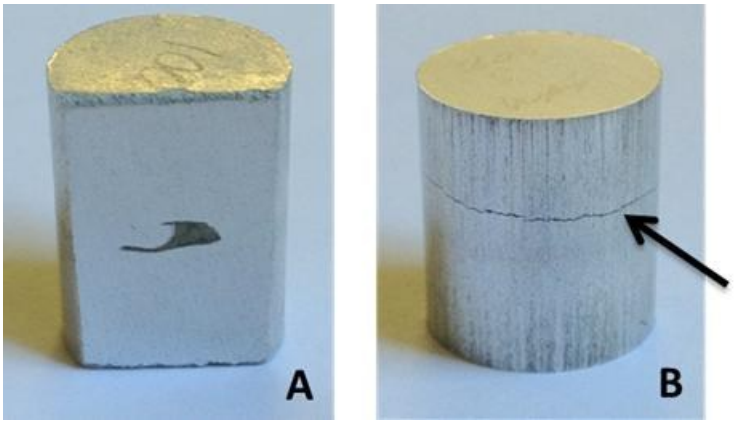

Figure 21: A: Cross sectioned internal structure compact (100 MPa compaction pressure, 9.53 mm diameter internal structure) with soft polyurethane foam fill. B: Epoxy fill internal structure compact (200 MPa compaction pressure, 6.35 mm diameter internal structure) with arrow indicating cracking.

Based on the initial developments, stearic acid fill with a 6.35 mm diameter cavity was selected as the basis for this work as this combination yielded the most consistent qualities. This combination functioned because it provided a compatible match between sphere size, internal structure size, and structure fill. The internal structure fill has to be selected to closely match the compliance of the powder to allow for uniform powder compaction across the entire compact. Relatively stiff fill materials such as epoxy restrict powder flow and have an increased spring back effect which result in cracking after ejection. Conversely, more compliant fill materials such as soft foams are usually able to match the powder compliance; however, they do not have the strength to stand up to compaction pressures. The internal structure size has to be selected to allow for powder densification as the minimum powder cross section. Larger structure sizes restrict powder flow in this region which results in poor densification and thus a weakened compact in this region. Additionally, the issue of selecting structure size, fill, and powder type becomes more complicated than just matching compliance based on the compaction pressure because material properties such as density, strength, and stiffness are constantly changing across all compaction pressures.

5.2 Visual Comparison

From the results obtained in from the preliminary testing discussed in the previous section, Figure 22 shows a comparison between an internal structure compact (left) and a conventional PM compact (right). It can be seen form this figure how the internal structure is completely encased in a compacted powder matrix. Theses samples are sectioned through the center and mounted in epoxy.

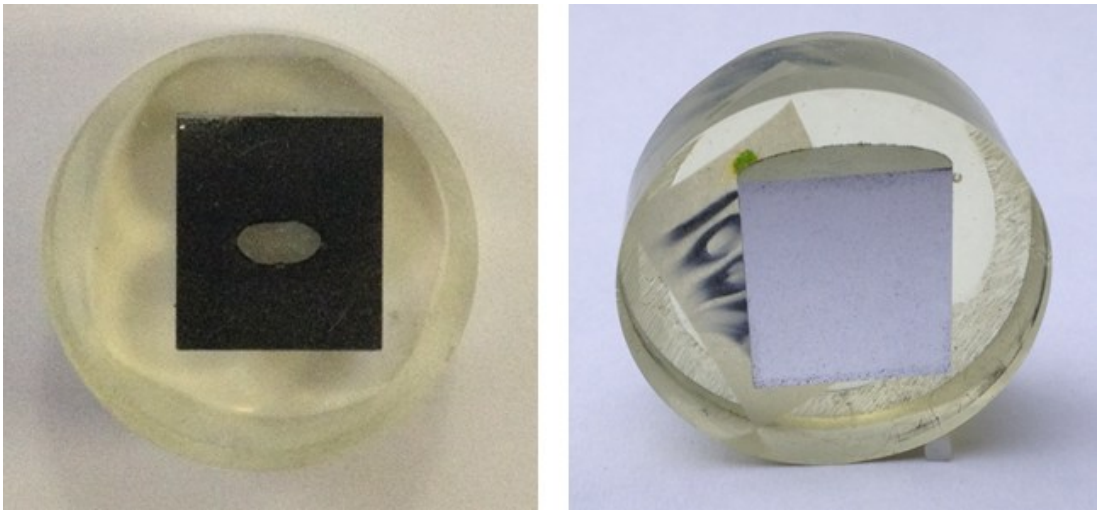

Figure 22: Internal structure compact (right) and conventional compact (right) compacted at 100 MPa, mounted in epoxy and sectioned along the mid plane.

5.3 Bulk Density

The bulk density of the internal structure compacts were compared to that of conventional PM samples of the same H/D ratio, shown in Figure 23. The bulk compaction curve of the internal structure samples compared to conventional Alumix 321 cylindrical compacts; the density of wrought aluminum (Al) is also plotted for reference. For each data point an average of five samples is reported, complete data for the compaction curve is given in Appendix B. Interestingly, the internal structure samples yield a somewhat constant reduction in density of 0.055 g/cc from 300 MPa to 400 MPa; however, initially at 100 MPa, the reduction in density afforded by the internal structure sample is quite small, only 0.029 g/cc.

Additional density analysis was performed on actual powder densification as shown in Figure 24. This plot shows the relative density of the conventional PM compact compared to the powder densification (not including the internal structure) of the internal structure compact. The relative density of the conventional PM samples was calculated as a percentage of wrought Al density. The powder densification of the internal structure compact was calculated in a similar fashion; however, the volume and mass of the structure and structure fill

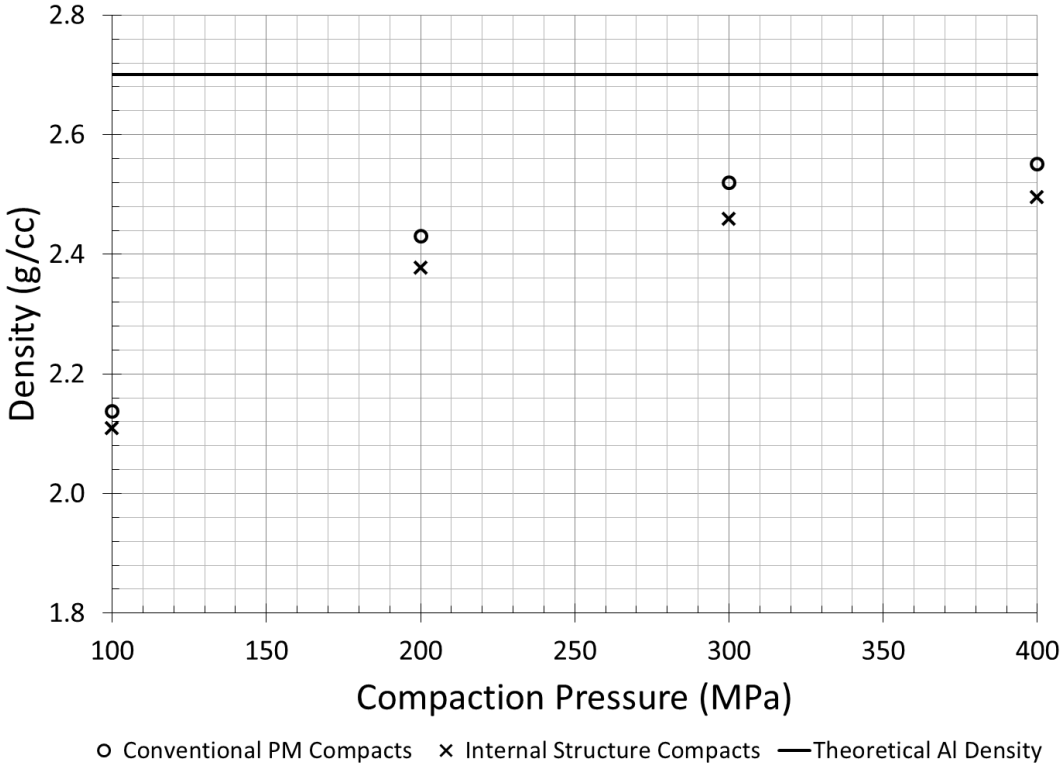

Figure 23: Compaction curves for internal structure compact (red) and conventional compacts (blue). An average of five samples is reported for each data point.

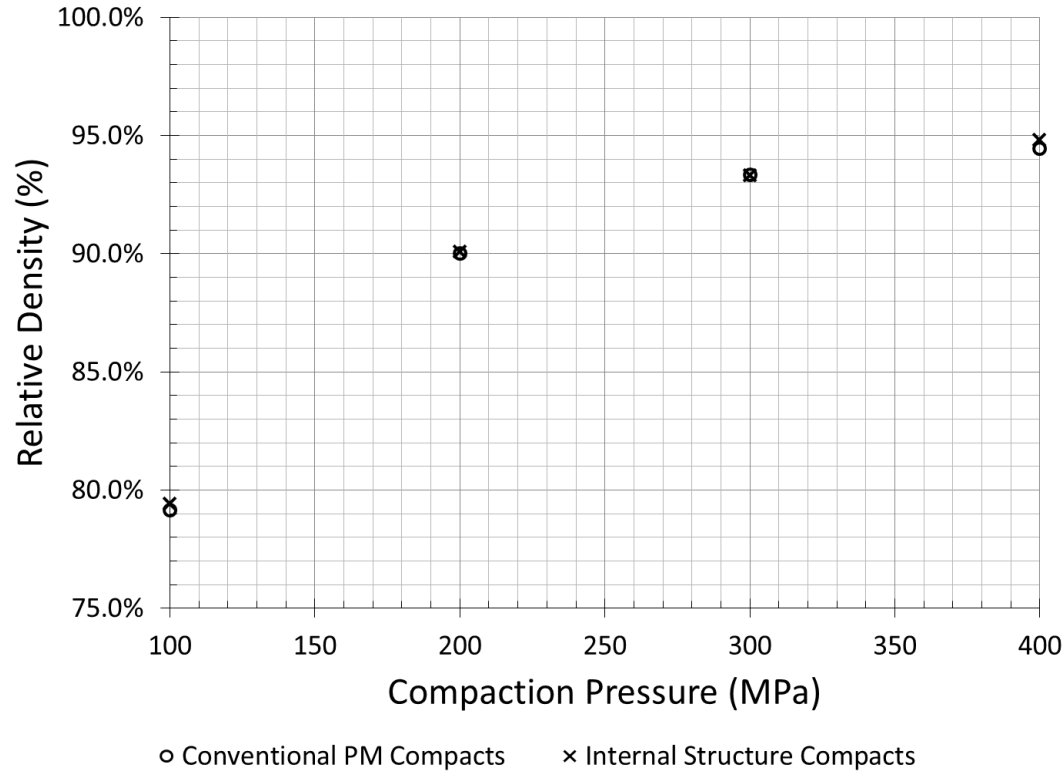

Figure 24: Powder densification in terms relative density of conventional PM compacts and internal structure compacts.

(assumed to be constant during the compaction process) were removed from the density calculations.

Interestingly, the internal structure compacts yield similar overall powder densification as the conventional PM compacts while maintaining a lower bulk density. This indicates that the lower bulk density of the internal structure (compared to the conventional PM compact) is directly a result of the internal structure density.

5.4 Optical Densitometry

The internal density gradients were analyzed using optical densitometry to determine the differences in density gradients between the internal structure compact and conventional PM compacts.

Shown in Figure 25 and Figure 26 are the density distributions with the internal structures and conventional compacts, respectively. The density plots start and 100 MPa on the left followed by 200, 300 and 400 MPa, each density plot represents half the sample. Generally, all the compacts show increasing density from 100 to 400 MPa, similar to the compaction curve in Figure 23.

All of the samples shown in Figure 25 and Figure 26 display a low density ring in the bottom outside corner characteristic of single action as described by German (2005) (see Figure 6); however, the internal structures compacts produced some interesting densification results in comparison to the conventional compacts; this is especially so at 100 MPa. Figure 27 shows the densification of internal structures and conventional compacts mirrored about the center line.

The 100 MPa internal structures compact shows sharp density gradients from top to bottom as compared to the conventional compact. Although, both compacts exhibit low density areas at the top and bottom of the compact, the internal structure compact exhibits a more intense high density region surrounding the internal structure. Alternatively, the conventional compact showed more uniform densification across the compact. It is particularly interesting that this high density region is clearly visible on the polished compact (seen in Figure 28) where arrows A and C highlight the low density areas and B highlights the high density area surround the internal structure.

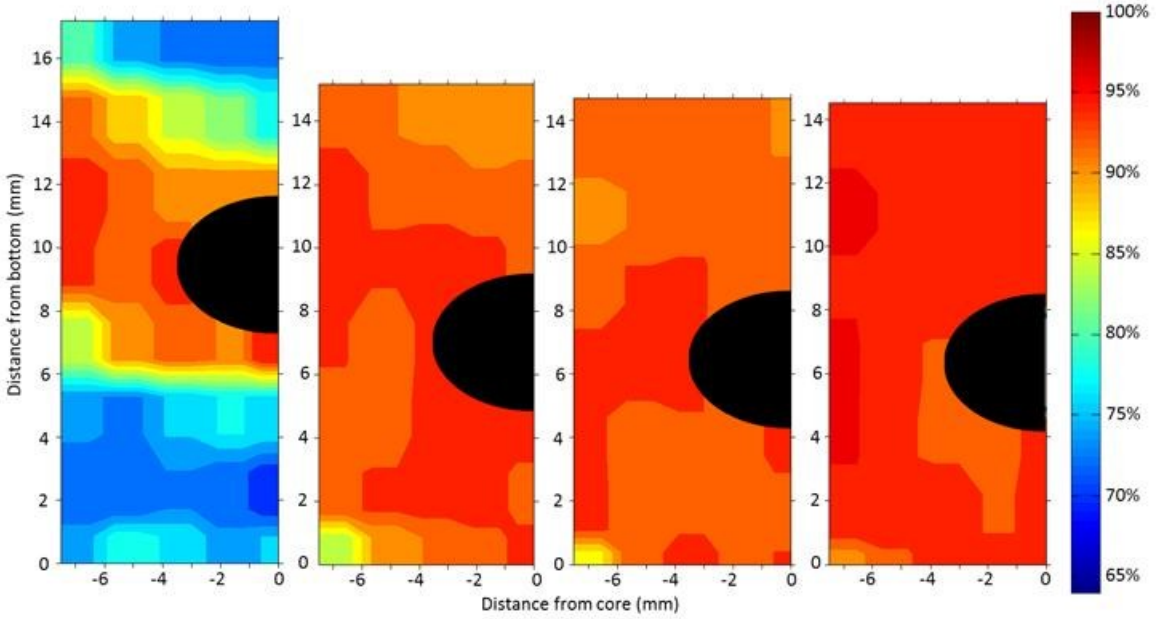

Figure 25: Density gradients of internal structures compacts. Compaction pressures from the left at 100, 200, 300, and 400 MPa. The black oval represents the internal structure. Scale on the right indicates percent relative density of wrought aluminum (2.70 g/cm³)

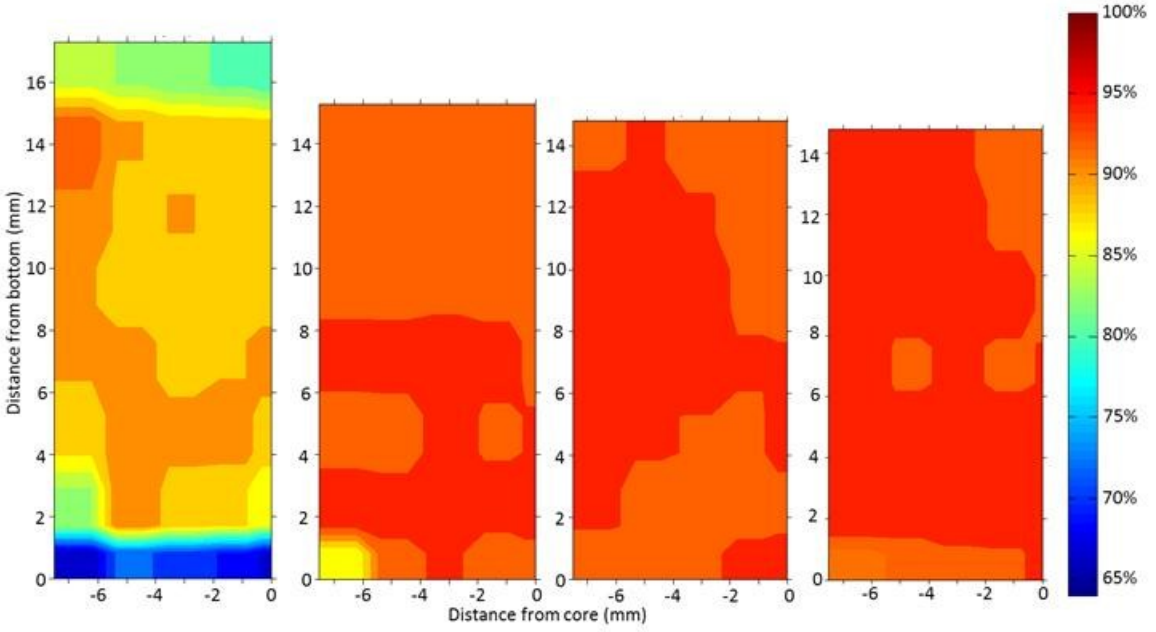

Figure 26: Density gradients of conventional PM compacts. Compaction pressures from the left at 100, 200, 300, and 400 MPa. Scale on the right indicates percent relative density of wrought aluminum (2.70 g/cm³).

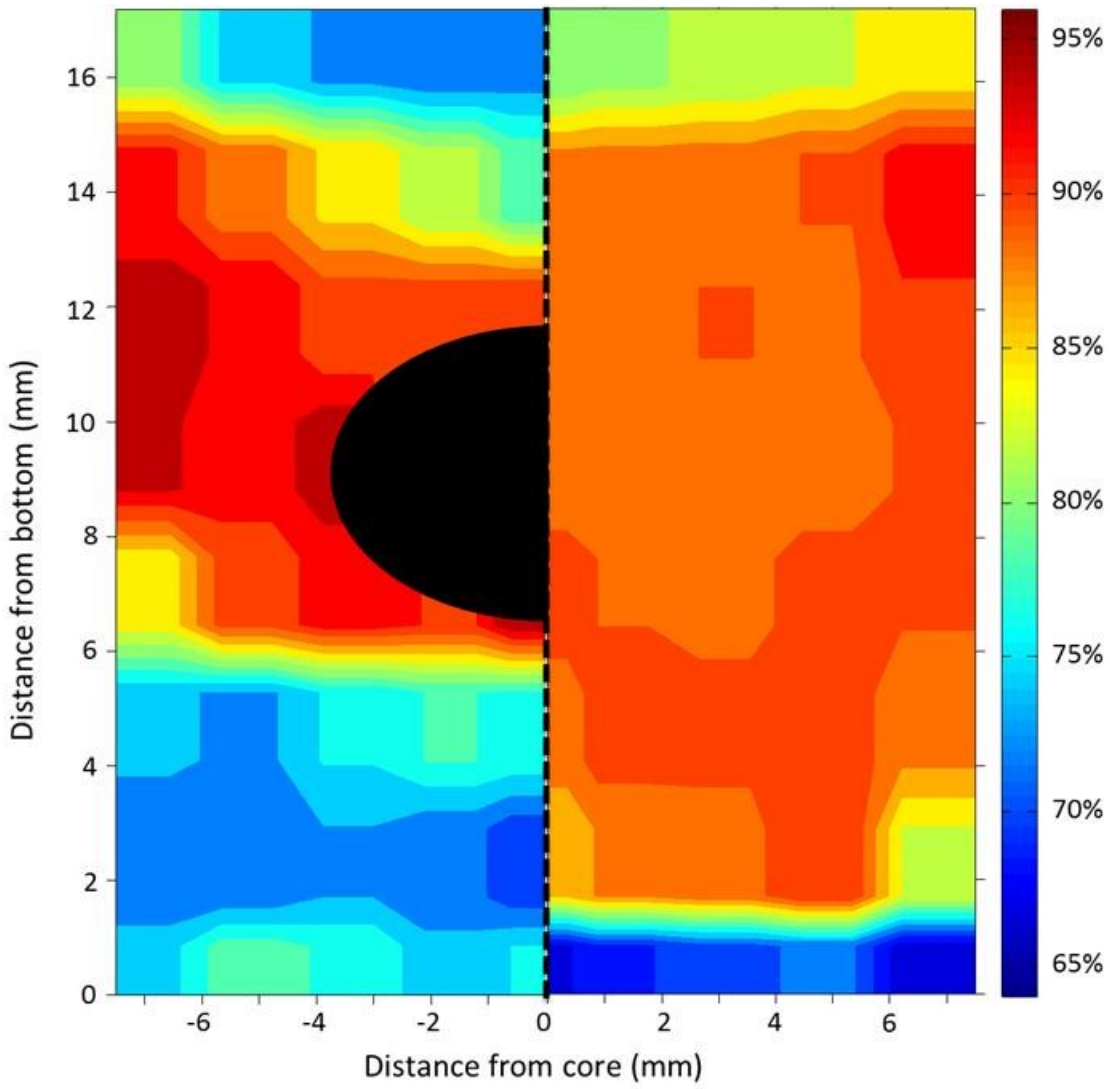

Figure 27: Density gradients of an internal structures compact (left) and a conventional PM compact at (right) at 100 MPa. Scale on the right indicates percent relative density of wrought aluminum (2.70 g/cm³).

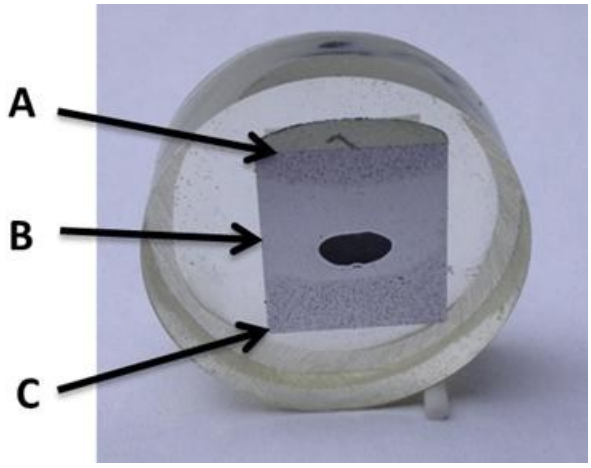

Figure 28: Internal structure compact (100 MPa) showing low density areas (arrows A and C) and the high density band surround the internal structure (arrow B).

This higher localized densification (Figure 28, arrow B) is most likely rooted in the stress concentration induced by powder flow and the internal structure geometry. During compaction, the powder attempts to flow around the internal structure which would induce additional pressure. This is because increased particle friction (as a result of more powder flowing through a smaller area) would slow powder flow and thus increase pressure, which in turn increases density. This result is compounded as the compaction pressure increases as more powder is forced into the area between the internal structure and the die wall. The increased densification and increased compaction pressure is to some degree a positive feedback event which causes the localized densification around the internal structure.

The localized high density band seen in the 100 MPa internal structure compact is a exceptional result for PM die compaction. The internal structure has afforded higher localized densification than a conventional PM compact at equal compaction pressure. This in itself presents several unique opportunities and practical advantages of the internal structure compact. Firstly, it would be possible to run a compaction press at lower pressures and obtain equal densification as a conventional compact compacted at higher pressures. Furthermore, the internal structure presents opportunities for strategic densification allowing for increased strength as a result of higher densification in targeted areas.

The density gradient trend of low density at the top and bottom, enclosing a high density ring in the middle of the compact shown at 100 MPa is still visible at 200 MPa (shown in Figure 29); however, the density gradients are greatly reduced. The measurements range from 84% to 96% relative density for 200 MPa; the range for 100 MPa is nearly three times greater, 65% to 95% relative density.

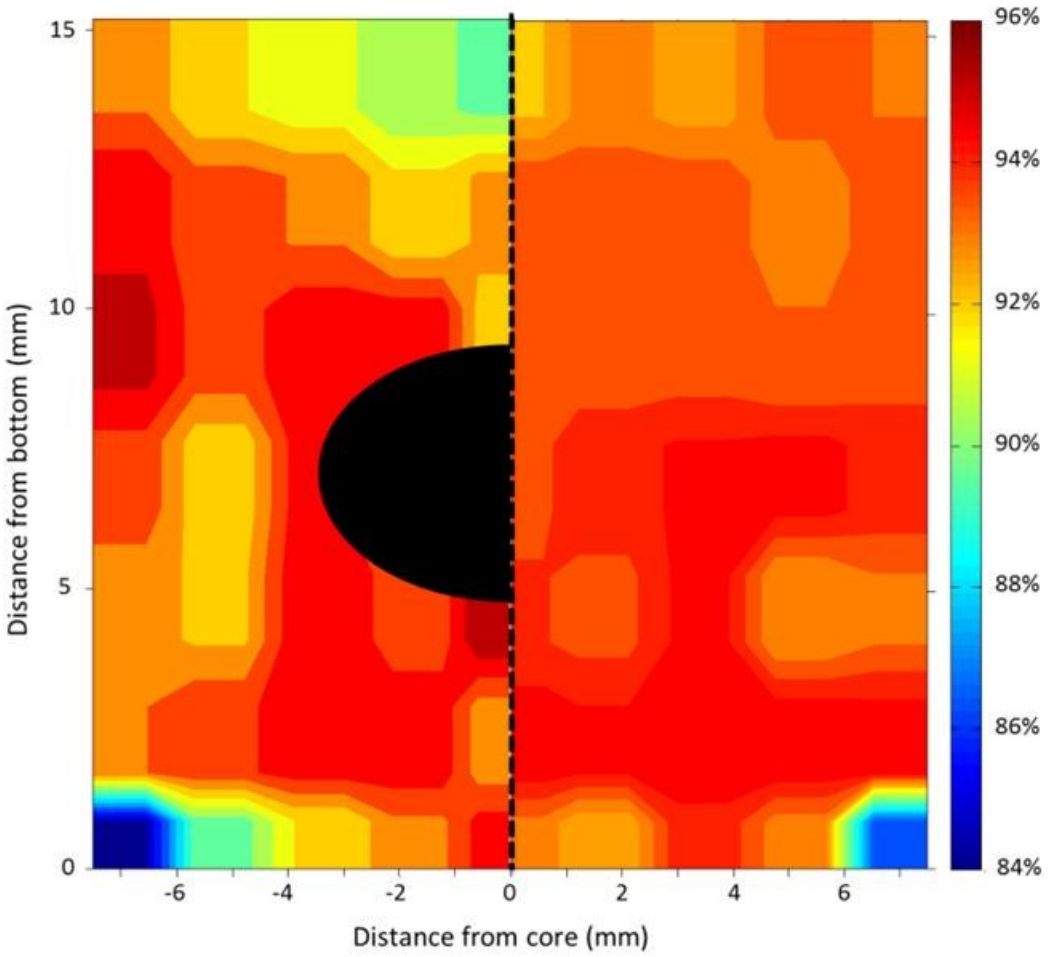

Figure 29: Density gradients of an internal structures compact (left) and a conventional PM compact at (right) at 200 MPa. Scale on the right indicates percent relative density of wrought aluminum (2.70 g/cm³).

The internal structures compact at 200 MPa still shows low density regions at the top and bottom, but the high density region surrounding the internal structure has increased in density and size. However, the magnitude of the density gradients in the internal structure compact are still slightly larger than the conventional compacts. Nevertheless, the compaction pressure is high enough such that densification can occur under the internal structure resulting in much more uniform densification compared to the 100 MPa internal structure compact. Also, the low density ring located in the outside corner of the internal structure sample (as well as the conventional sample) at 200 MPa is strongly maintained compared to 100 MPa.

The additional densification from 200 MPa to 300 MPa is somewhat minimal; although, at 300 MPa (Figure 30) the high density area surrounding the internal structure has reduced in size as a result of the increasing density uniformity in the compact.

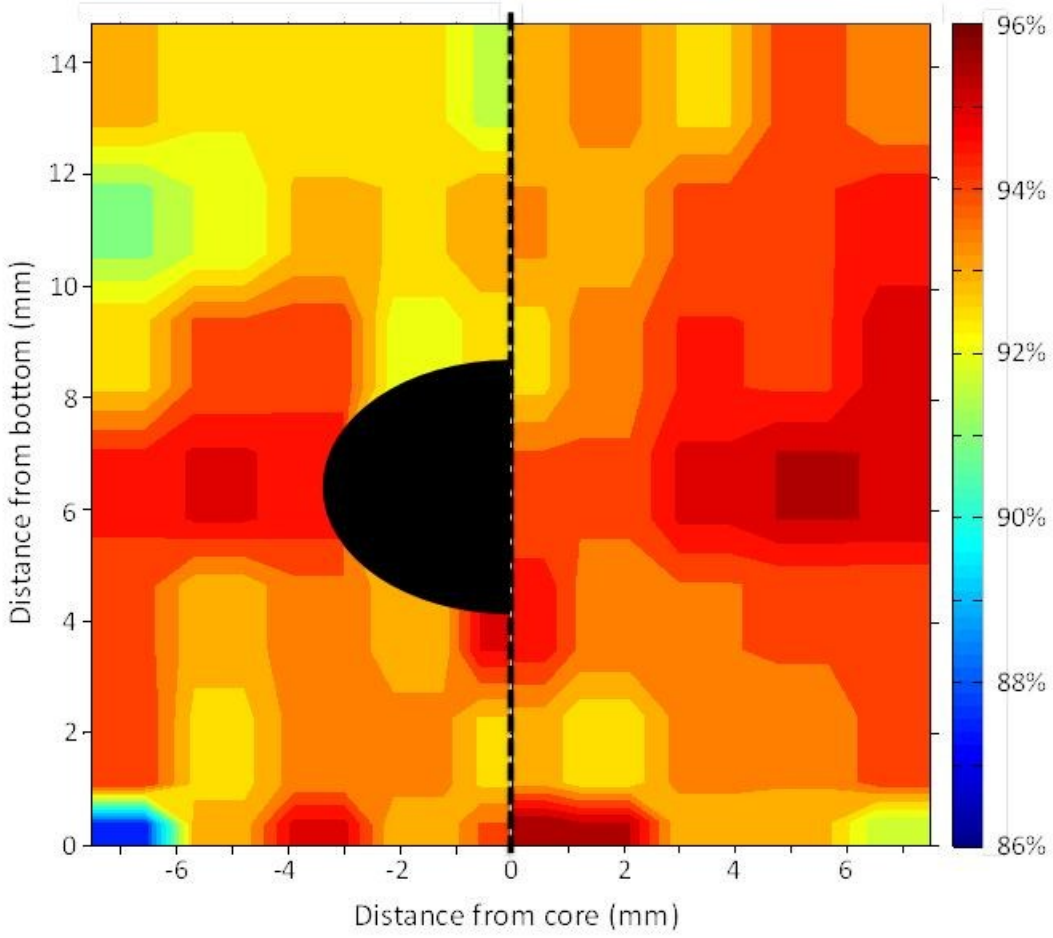

Figure 30: Density gradients of an internal structures compact (left) and a conventional PM compact at (right) at 300 MPa. Scale on the right indicates percent relative density of wrought aluminum (2.70 g/cm³).

Similar to the internal structure sample compacted at 300 MPa; the 400 MPa sample shows the high density area surrounding the internal structure migrating away from the internal structure, this is shown in Figure 31. Although the high density area has moved away from the internal structure, the density spread at 400 MPa; ranging from 96% to 90%, is still reduced from 300 MPa; ranging from 96% to 86%.

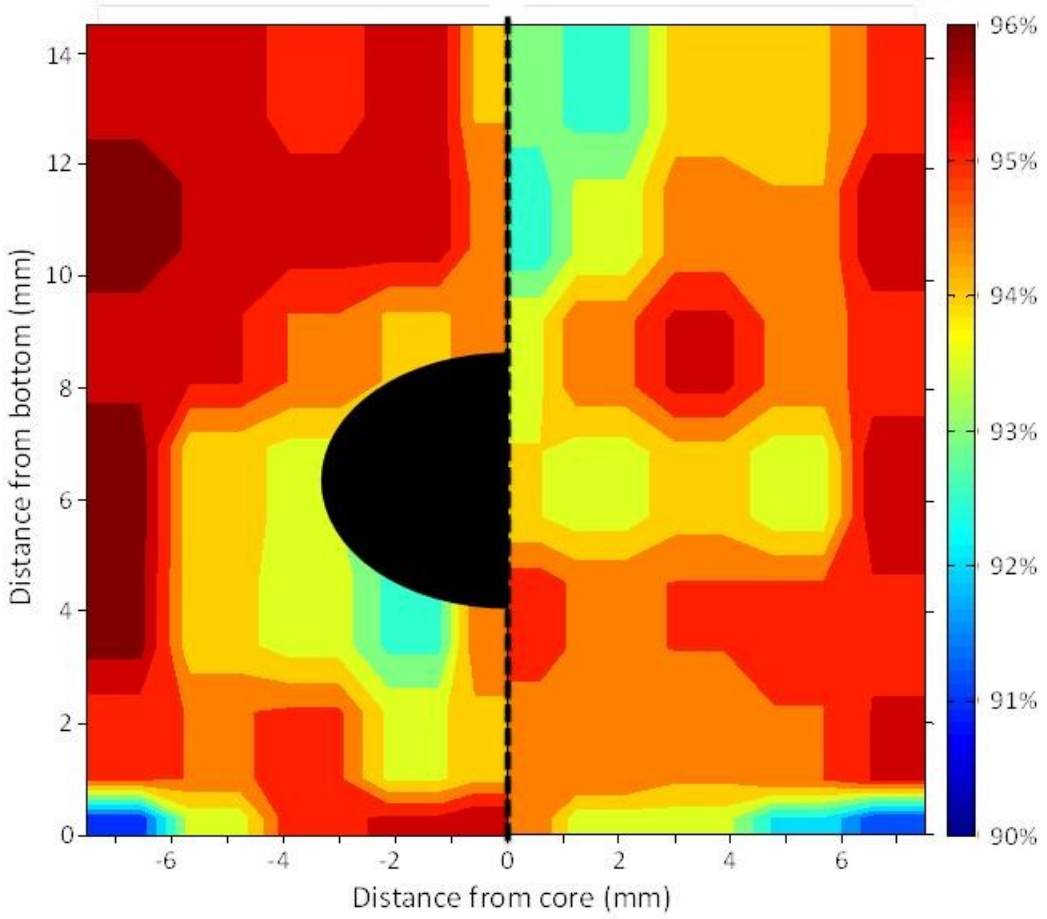

Figure 31: Density gradients of an internal structures compact (left) and a conventional PM compact at (right) at 400 MPa. Scale on the right indicates percent relative density of wrought aluminum (2.70 g/cm³).

Shown in the results above, the internal structure compacts drastically alter the densification and result in higher localized densities than conventional PM compacts for a given pressure. This was especially visible at 100 MPa compaction pressure (see Figure 27 and Figure 28) where it displayed a distinct high density band surrounding the internal structure. This presents the opportunity of possibly engineering the densification of a powder compact. In doing so preferential strength can be engineered while saving on material in area where it is not needed.

5.5 Compressive Green Strength

5.5.1 Experimental Results

Compressive green strength (CGS) testing was performed as per the methods outlined in Section 4.6 to determine how internal structures compared to conventional PM compacts. The green strength for the conventional PM samples follows an expected trend where the green strength increases with increasing compaction pressure (and thus increasing density) as shown in Figure 32. The internal structures samples follow this trend until a compaction pressure of approximately 300 MPa, after which (at 400 MPa) there is a plateau in green strength. It should be noted that each data point represents an average of four compressive green strength tests. The error bars represent plus/minus one standard deviation; complete CGS testing data is given in Appendix C.

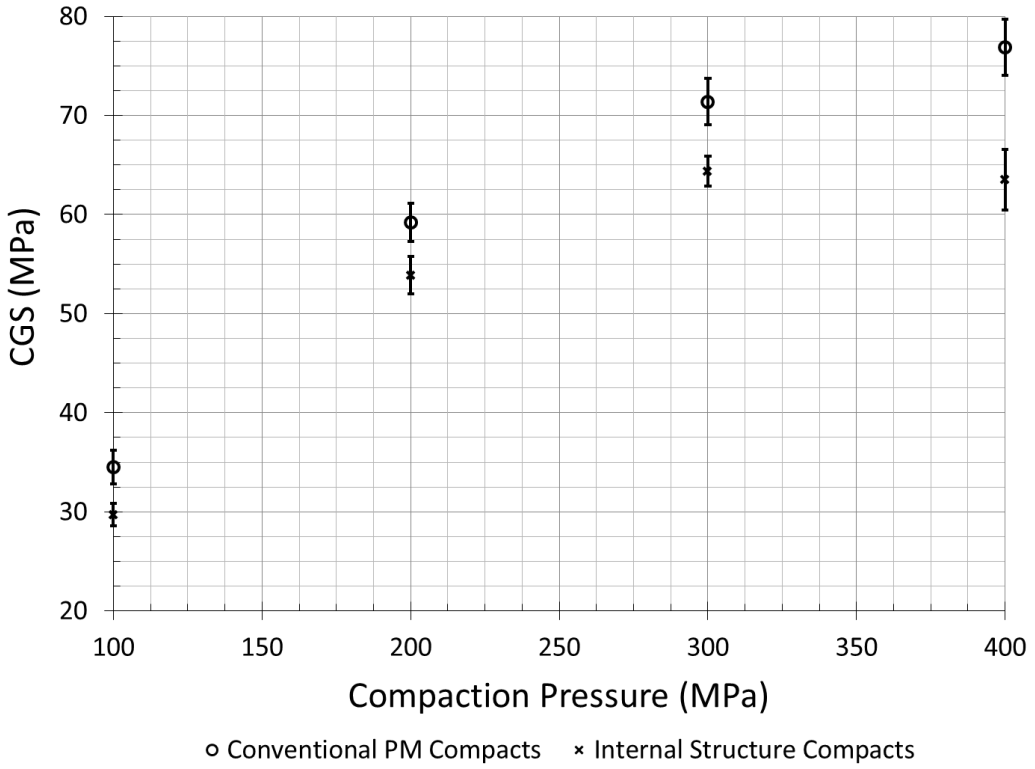

Figure 32: CGS testing for conventional PM samples (blue) and internal structure samples (red). Each data point is an average of four samples with the displayed error bars showing one standard deviation.

The most interesting result shown is that the CGS of the internal structure compact is maintained from 300 MPa to 400 MPa. Generally, it is expected that increasing compaction pressure and thus, increasing density result in better mechanical properties (Brewin, et al., 2010). For the case of the internal structure it is theorized that for this type of structure there is a green strength limit that occurs at in the region of 400 MPa. As a result of this unusual result further investigation is warranted, therefore a finite element model was developed.

5.5.2 Finite Element Model Development

A finite element (FE) model was created to be used as a tool to give an indication and evaluation of the events that occur during the compaction process of the internal structures compact in addition to helping to explain the plateau event of the internal structure compact CGS. Finite element simulations of the compaction process were performed using the FE hydrocode LS-DYNA version 971. A schematic of the compaction model geometry at the initial state is shown in Figure 33. The model, meshed using axi-symmetric elements consisted of upper/lower punches, die wall, powder, cavity shell and cavity fill were meshed using Altair Hyperworks 11.0. The upper/lower punches were assumed to be rigid bodies and made of steel. The powder employed a material model developed by Selig (2012) which accounts for the pressure-densification nature of metal powders. The internal structure was modeled using a simplified Johnson-Cook material model for aluminum attained from the U.S. Department of Transportation (Kay, 2003). Lastly, a material model was created for the stearic acid using *MAT_SOIL_AND_FOAM, this material model is simple in nature and was derived from material properties of stearic acid.

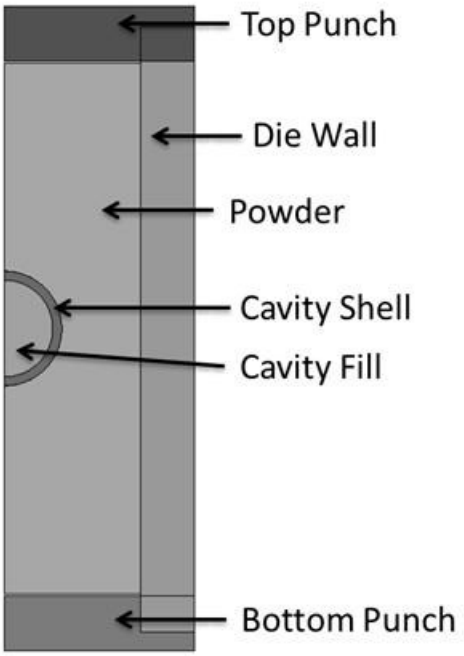

Figure 33: FE model of internal structure compaction.

The model was run using explicit time integration and employed displacement control of the upper punch to simulate single action compaction. The lower punch and the die wall were constrained in all directions while the upper punch was free to move axially but constrained in all other directions. The initial powder fill height was determined based on experimental testing. The complete code used for this simulation can be found in Appendix A.

5.5.3 Finite Element Model & Compressive Green Strength

The FE model was able to point to several potential phenomena that could cause the plateauing of the compressive strength. Firstly, there is an interesting evolution of shear stress surrounding the internal structure from 100 to 400 MPa. From Figure 34 we can see that as the compaction pressure increases, so does the shear stress surrounding the internal structure. This is especially seen from the 300 to 400 MPa increase in pressure as a large area of negative shear develops on the underside of the internal structure.

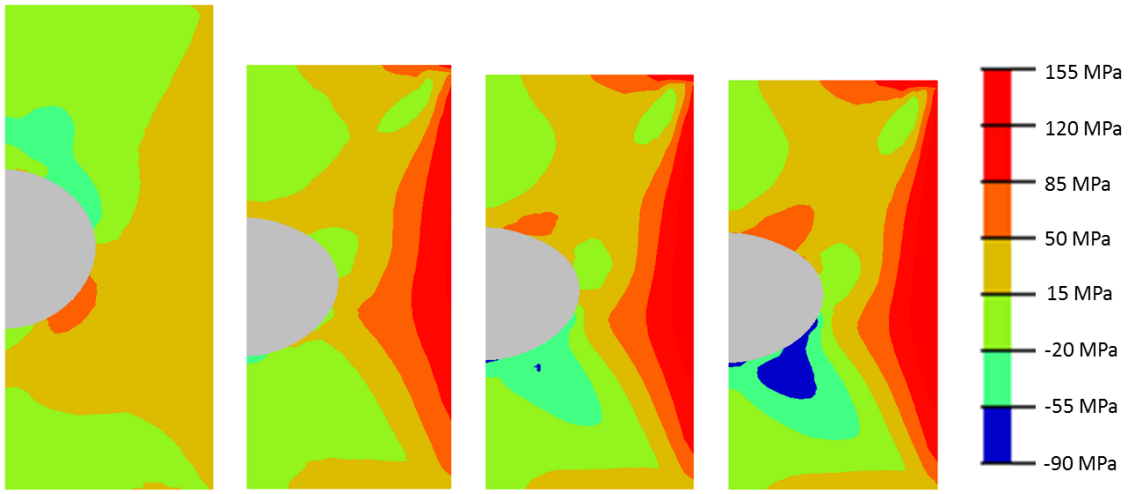

Figure 34: FE model of shear stress in the internal structures compacts at compaction pressures of 100 (left), 200, 300, and 400 MPa (right).

The increase in negative shear contributes to a large gradient between internal structure and the shear stress caused by die wall friction. This gradient, from negative to positive shear, would create a stagnate area of powder where the negative and positive shear stress vectors are in opposite directions, in turn creating a potential failure zone. Figure 35 illustrates the shear difference in the internal structures compact. An interesting feature of this plot is that at 300 and 400 MPa compaction pressure there is a large gradient stemming from the internal structure that protrudes out towards the top and bottom corners.

Thus, it is hypothesized that as the compaction pressure in a sample increases, the powder movement can become restricted and shear within the compact will develop (O'Brien & James, 1988). In the present case, pressures above 300 MPa there are two competing features that govern the strength of the internal structures compact: the compact density and the shear stress. Therefore, increasing the compaction pressure (and the density) causes the shear stress gradients within the compact to increase thereby creating a tradeoff point where the strength will maximize (plateau).

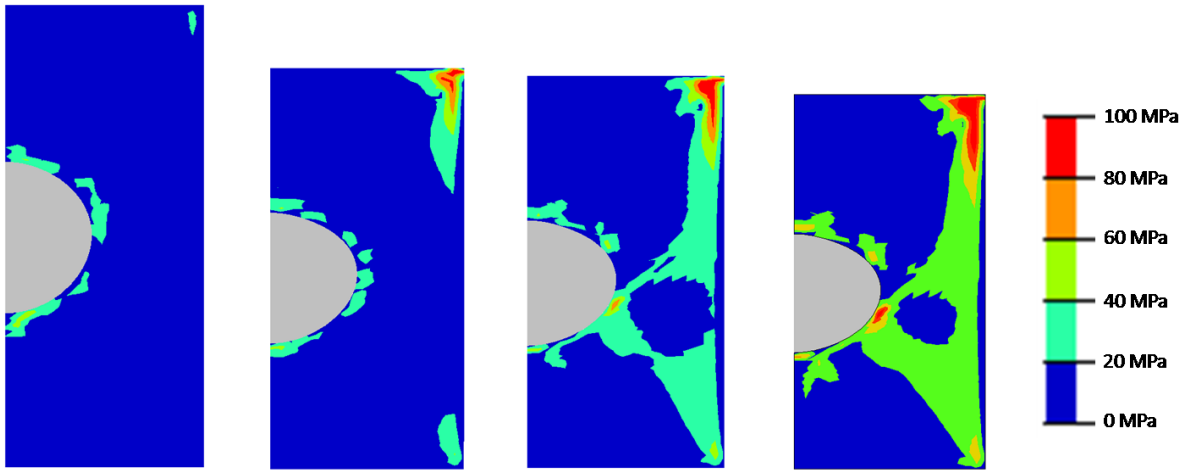

Figure 35: FE model of shear stress difference in the internal structures compacts at compaction pressures of 100 (left), 200, 300, and 400 MPa (right). The die wall as well as top and bottom have been removed for viewing purposes.

The failure of the internal structures samples failed along the shear gradient areas illustrated in Figure 35, the actual failure is shown in Figure 36. The failure area, located between the areas of negative and positive shear stress, of the internal structure compact matches quite closely to the failure area predicted by analyzing the FE model results.

By comparison, the conventional samples show the classic shear failure through the compact at roughly a 45° angle, shown by the arrow in Figure 37. The internal structure samples exhibit a similar shear stress failure; however, it is in a distinctly different area.

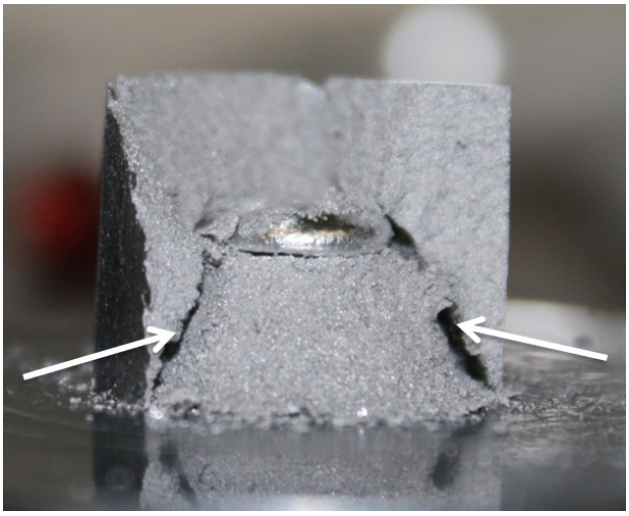

Figure 36: Failure of internal structure compacts from CGS testing with initial compaction pressure of 400MPa.

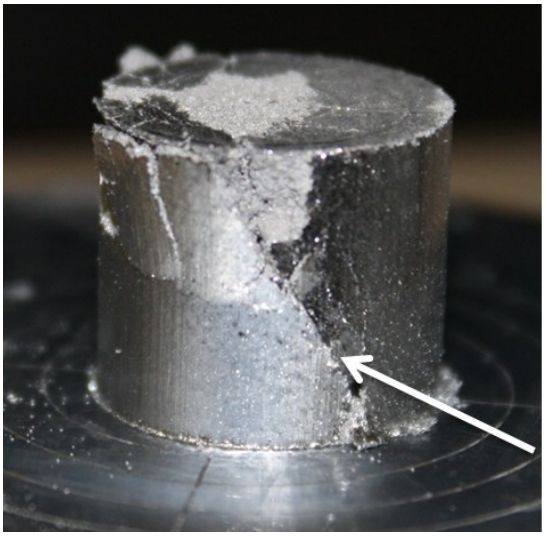

Figure 37: CGS testing failure indicated by the white arrow of conventional PM sample compacted at 400 MPa.

Chapter 6: TECHNOLOGY DEVELOPMENTS

As an extension of the core investigation and the results found, two additional areas of interest were examined: determining a preliminary path of research for creating a hollow internal structure and sintering the internal structure compacts.

6.1 Hollow Structures

The current state of the internal structure technology allows for compaction with a solid fill; however, the structure shell does not have enough strength to undergo compaction in a hollow state to allow a hollow internal in just the compaction step. Thus, an additional heating phase post compaction was devised in an attempt to remove the stearic acid contained within the internal cavity; this is illustrated in Figure 38.

The compaction process is performed at room temperature; however, at the end of the compaction cycle the pressure is maintained as heat is applied to the die, by way of a heating jacket. During the heating phase the compaction pressure is slowly lower as the stearic acid melts. The two tests that were performed for the preliminary study are summarized in Table 10.

Table 10: Preliminary study on heating conditions for creating hollow internal structures.

Compaction Pressure (MPa)	Steady state heating temperature (°C)	Heating Time (min)
100	90	40
300	90	40

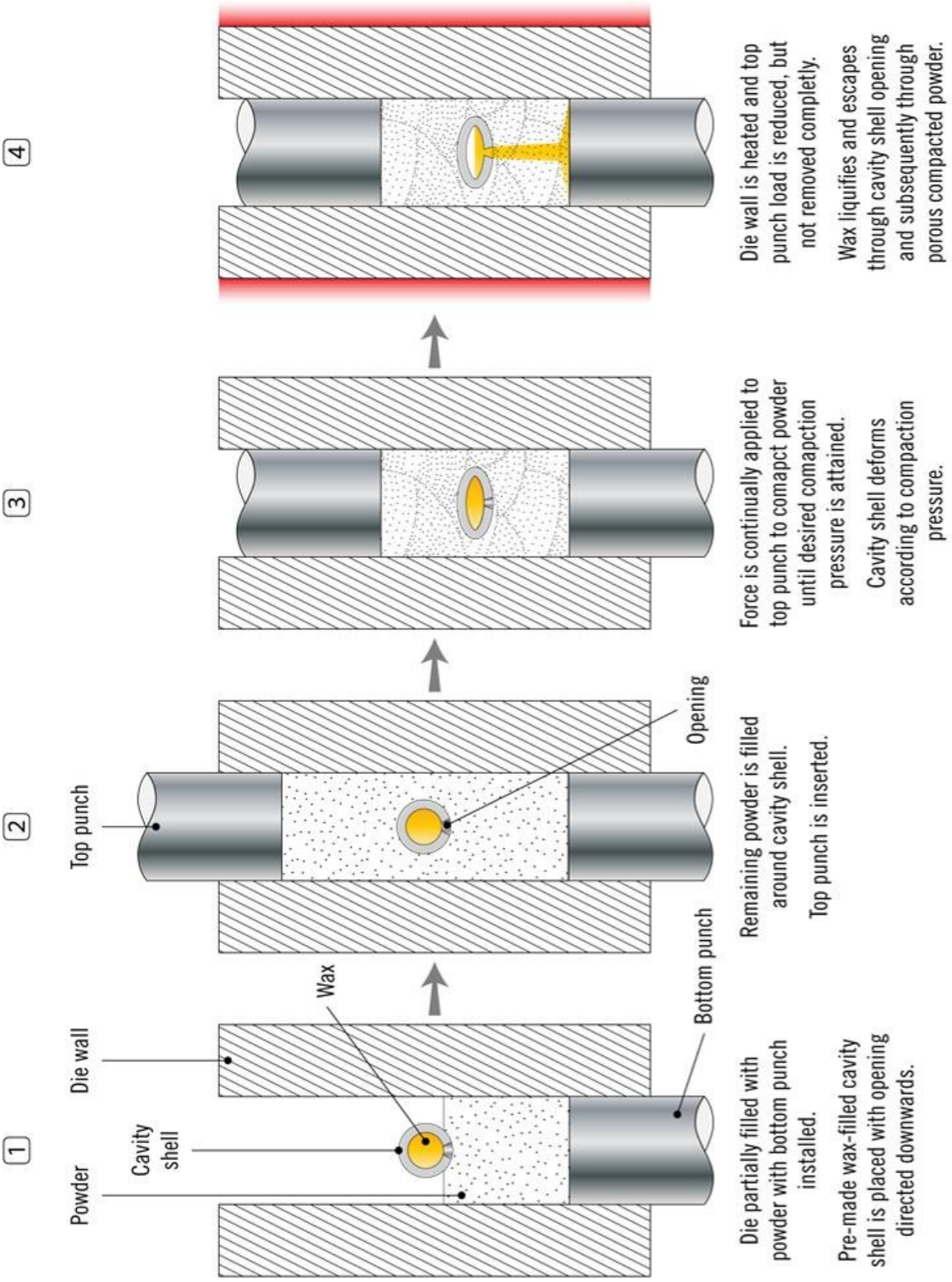

Figure 38: Compaction process of the internal structure with an additional heating phase to allow for the removal of stearic acid.

The initial results of creating hollow internal structures are shown in Figure 39 which shows a stearic acid filled structure compacted at 100 MPa (A) in comparison to samples compacted with the additional heating phase at 100 (B) and 300 MPa (C).

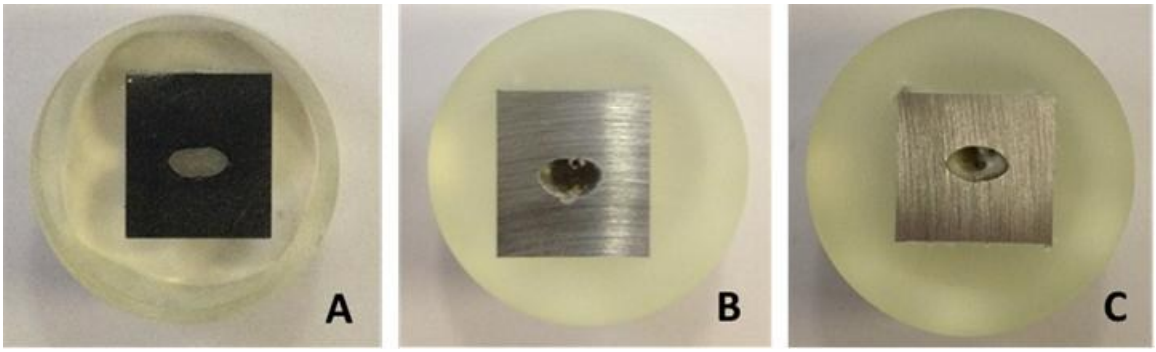

Figure 39: Comparison of stearic acid filled structure compacted at 100 MPa (A) to internal structure samples compacted with an additional heating phase at 100 (B) and 300 MPa (C).

The sample compacted at 100 MPa with the additional heating phase showed complete removal of the stearic acid contained within the sample. The sample compacted at 300 MPa showed some stearic acid removal, but not to the extent of the 100 MPa. It is believed that the reduced porosity at 300 MPa restricted the flow of stearic acid and did not allow for complete removal. It is hoped that during sintering the elevated temperatures will allow for more of a burn off of the stearic acid rather than melting experienced in this testing.

6.2 Sintering Internal Structure Compacts

Hollow and stearic acid filled internal structure samples were sintered in an effort to evaluate their respective sintering responses. For each instance, (hollow and stearic acid filled) samples were compacted at 100 and 300 MPa and sintered in a Lindberg® Blue M® three-zone tube furnace. Lubricant burn off was performed at 400ºC for 20 minutes and sintering was performed at 630ºC for 20 minutes in a nitrogen atmosphere where the complete sinter temperature profile is given in Appendix D.

Internal structure samples with stearic acid fill, both 100 and 300 MPa, resulted in cracking during sintering. This is most likely a result of the stearic acid expanding rapidly during the initial heating stages of sintering. This causes the sample to separate around the internal structure as shown in Figure 40.

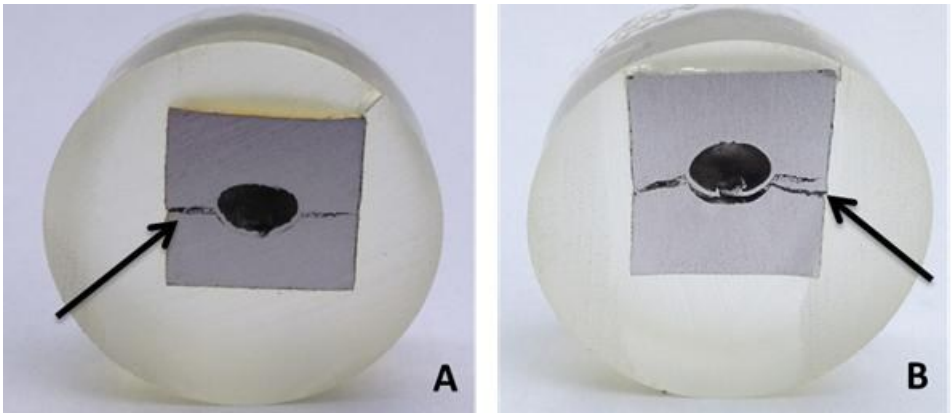

Figure 40: Stearic acid filled internal structure samples (A: 100 MPa compaction pressure, B: 300 MPa compaction pressure) post sintering. Arrows are indicating cracks that formed during the sintering process.

Hollow internal structure samples showed encouraging results in that no cracks were observed in the 100 MPa sample after sintering which is shown in Figure 41 A. The hollow internal structure compacted at 300 MPa showed a slight crack (Figure 41 B indicated by the arrow) which was most likely formed as a result residual was left after the post compaction heating process (see Figure 39 C).

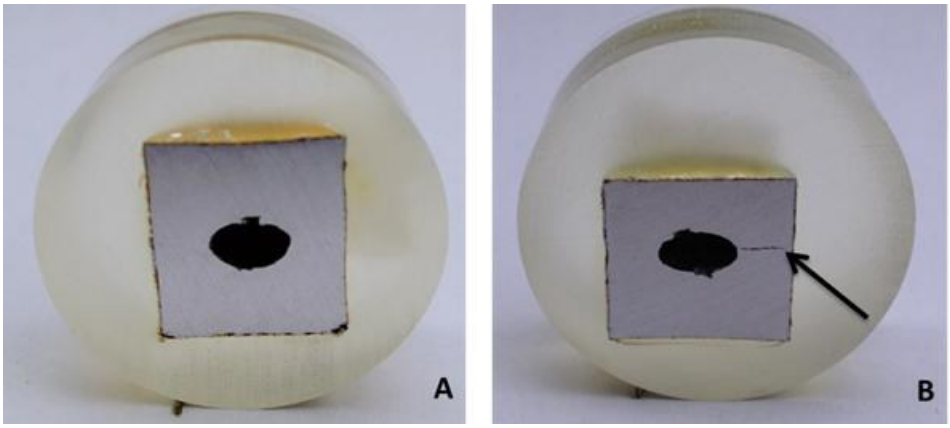

Figure 41: Sintered hollow internal structure samples (A: 100 MPa compaction pressure, B: 300 MPa compaction pressure) sectioned along the mid plane.

Chapter 7: CONCLUSIONS & RECOMMENDATIONS

7.1 Conclusions

This research contributed several important technological developments to the manufacture of internal structure compacts using die compaction. A complete review of internal structure compacts was completed detailing the current performance and state of development of these components and most importantly; a new method of manufacturing green PM compacts with internal structures has been developed and analyzed.

An internal structure compact was developed using die compaction of Alumix 321 and stearic acid filled aluminum 3003 sphere. The internal structure compact showed interesting results in that preferential densification occurred around the internal structure. This could potentially allow for engineering densification within a compact by strategically placing internal structure in areas where increased strength is required. Although positive results were obtained in terms of densification, internal structure compact suffered from increasing internal shear gradients at high compaction pressures resulting in limited CGS at 400 MPa.

Two additional developments of the internal structure compact were considered: a hollow internal structure and sintered internal structure compacts. The hollow internal structures showed promising results at 100 MPa, however; at 300 MPa the density of the compact was too high to allow the stearic to expel from the compact. The stearic acid filled spheres showed poor results during sintering as the samples formed large cracks during sintering. The hollow samples showed better sintering results in that the 100 MPa compact showed no flaws, however; the 300 MPa sample formed a slight crack post sintering.

7.2 Recommendations

The compaction methodology to produce green PM compacts containing internal structures has been completed and several important findings have been discovered however; given how novel this research is, there are four important areas that can be addressed to further the development of internal structure compacts: different internal structure shapes, the development of hollow internal structures, sintering procedures, and validating the FE model of the compaction process.

Firstly, other internal structures should be evaluated to test the limits of the technology as well as targeting novel uses. This includes evaluating different internal shapes/sizes, (in addition to the sphere tested in the work) and various fill types. Different internal shapes will most certainly result in different characteristics such as bulk density, density distributions and green strength. In addition to the internal structure shape, the structure fill types will most certainly result in different physical compact characteristics. It is important to evaluate these characteristics because they can be used to engineer PM components with preferential high or low density areas, or be used to engineer high strength PM components.

Secondly, a method of producing hollow internal structures should be evaluated in greater detail. Preliminary testing has begun to produce hollow internal structures by removing the stearin contained within the internal structure prior to sintering. Such things as ideal burn off temperature and time have yet to be determined, however; other methods of producing hollow internal structures compacts should be evaluated; this could include metal foam or rapid prototyped structures.

Thirdly, sintering profiles and the reaction of powder and core material has to be researched to determine the reaction between internal structure and the powder matrix. As sintering is

a multi-dimensional subject, the internal structure further complicates the process as there are two different materials interacting within the compact. Preliminary sintering tests were performed with positive results however the process needs further refinement.

The FE model developed for the research conducted in this work proved to be valuable in in showing phenomena intrinsic to the compaction process of the internal structures. However, it would be useful to fully validate the FE model to allow for the design and testing of new internal structures while saving time with experimental research.

REFERENCES

Aluminum Association, T. (2008). Alcoa Earns 'Casting of the Year' Award for BMW Rear Control Arm Retrieved June 21, 2012, from http://www.aluminum.org/AM/Template.cfm?Section=Home&template=/CM/HTMLDisplay.cfm&ContentID=21373

Andersen, O., Hungerbach, W., Stephan, G., & Studnitzky, T. (2007). inno.zellmet - a concerted approach towards the application of non-foam type cellular metals. *Thermec 2006, Pts 1-5, 539-543*, 1892-1897.

Andersen, O., Waag, U., Schneider, L., Stephani, G., & Kieback, B. (2000). Novel metallic hollow sphere structures. *Advanced Engineering Materials, 2*(4), 192-195.

ASTM. (2003). ASTM B328-96 *Standard Test Method for Density, Oil Content, and Interconnected Porosity of Sintered Metal Structural Parts and Oil-Impregnated Bearings*: ASTM.

Augustin, C., & Hungerbach, W. (2009). Production of hollow spheres (HS) and hollow sphere structures (HSS). *Materials Letters, 63*(13-14), 1109-1112.

Beck, G., Selig, S., Doman, D. A., & Plucknett, K. (2011). *Densitometry Analysis to Determine Density Distribution in Green Compacts*. Paper presented at the International Conference on Powder Metallurgy & Particulate Materials, San Francisco.

Belhadjhamida, A., Williams, D., & Davies, J. (2011). US20110070119A1. U. S. P. Office.

Brewin, P., Coube, O., Doremus, P., & Tweed, J. (2010). *Modelling of Powder Die Compaciton*: Springer.

Capus, J. (2011). Powder metallurgy, progress and the eco-friendly car. *Metal Powder Report*, 16-18.

Dale, J. R. (2011). Sustainability Manufacturing within the Pm Industry. *International Journal of Powder Metallurgy, 47*(1), 23-25.

Donaldson, I. W., T.E. Geiman, and R.K. Williams. (2011). *A novel approach for manufacturing powder-forged connecting rods*. Paper presented at the 2011 Conference on Powder Metallurgy & Particulate Materials, San Francisco.

Fang, Z. Z. (2010). Powder metallurgy titanium—Challenges and opportunities. *International Journal of Powder Metallurgy, 46*(5), 9-10.

Geiger, C. F. (1946). United States Patent No. 2553759. U. S. P. Office.

German, R. M. (2005). *Powder metallurgy and particulate materials processing : the processes, materials, products, properties and applications*. Princeton, New Jersey: Metal Powder Industries Federation.

Granules, E. (2012). ECKA Alumix Typical Chemical Composition, Physical Characteristics, and Sintered Properties, from http://www.ecka-granules.com/index.php?id=153&typ=15&anwendung=3&L=2.

Greune, C. (1989). United States Patent No. 4867412. U. S. P. Office.

Gruver, J. H. (1917). United States Patent No. 1278917. U. S. P. Office.

Guyoncourt, D., Tweed, J., & Gough, A. (2001). Constitutive Data and Friction Measurements of Powders using Instrumented Die. *Powder Metallurgy, 44*(1), 23-33.

Haggblad, H. A., & Oldenburg, M. (1994). Modeling and Simulation of Metal-Powder Die Pressing with Use of Explicit Time Integration. *Modelling and Simulation in Materials Science and Engineering, 2*(4), 893-911.

Hall, I. W., Guden, M., & Yu, C. J. (2000). Crushing of aluminum closed cell foams: Density and strain rate effects. *Scripta Materialia, 43*(6), 515-521.

Hollomet. (n.d.). globomet Retrieved January, 28, 2012, from http://www.hollomet.com/cms/produkte/globomet.html?L=1

Isometall. (n.d.). Ball Manufacturing Process Retrieved January 31, 2012, from http://www.isometall.de/kugelherstellung.htm

Kandeil, A., Demalherbe, M. C., Critchley, S., & Dokainish, M. (1977). Use of Hardness in Study of Compaction Behavior and Die Loading. *Powder Technology, 17*(3), 253-257.

Kay, G. (2003). *Failure Modeling of Titanium 6Al-4V and Aluminum 2024-T3 with The Johnson-Cook Material Model.* (DOT/FAA/AR-03/57). Washington DC.

Levinstein, M. A., & Butts, W. R. (1969). United States Patent No. 3466166. U. S. P. Office.

Li, W. X., Nam, J., & Lannutti, J. J. (2002). Density gradients formed during compaction of bronze powders: The origins of part-to-part variation. *Metallurgical and Materials Transactions a-Physical Metallurgy and Materials Science, 33*(1), 165-170.

Lutheran, M. E. (2011). State of the PM industry in North America—2011. *Advances in Powder Metallurgy & Particulate Materials, 47*(4), 45-48.

Ma, L., Zahrah, T., & Fields, R. (2004). Numerical three dimensional simulation of cold compaction and springback for prealloyed powder composites. *Powder Metallurgy, 47*(1), 31-36.

Martin, A., Knight, R., & Ellis, G. (1961). The Forming of Hollow Shapes in Beryllium By Loose Sintering and Hot Pressing. *Powder Metallurgy*(7), 268-282.

MatWeb. (2012). Alclad Aluminum 3003-O Retrieved April 18, 2012, from http://www.matweb.com/search/DataSheet.aspx?MatGUID=dbe8df6a132547b4982311b9698e63be&ckck=1

Mccabe, T. J., Godby, L. V., & Trasorras, J. R. L. (1994). Metallographic Sample Preparation Techniques and Image Analysis for Density Distribution Determination in Steel Powder Compacts. *Advances in Powder Metallurgy & Particulate Materials - 1994, Vol 2*, 175-183.

McGee, S. W., & Mikoda, J. H. (1975). U. S. P. Office.

Meluch, L. (2009). *Warm Compaction of Aluminium Alloy Alumix 123*. PhD, University of Birmingham.

Molinari, A., Santuliana, E., Cristofolini, I., Rao, A., Libardi, S., & Marconi, P. (2011). Surface modifications induced by shot peening and their effect on the plane bending fatigue strength of a Cr-Mo steel produced by powder metallurgy. *Materials Science and Engineering a-Structural Materials Properties Microstructure and Processing, 528*(6), 2904-2911. doi: 10.1016/j.msea.2010.12.072

Neville, B. P., & Rabiei, A. (2008). Composite metal foams processed through powder metallurgy. *Materials & Design, 29*(2), 388-396.

Nguyen, C. (1992). United States Patent No. 511729. U. S. P. Office.

Novak, P. J. (1972). United States Patent No. 3691704. U. S. P. Office.

O'Brien, R. C., & James, W. B. (1988). *A Review of Nondestructive Testing Methods and Their Applicability to Powder Metallurgy Processing*. Paper presented at the International Powder Metallurgy Conference and Exhibition.

O'Neil, M. J. (2006). *The Merck index : an encyclopedia of chemicals, drugs, and biologicals* (14th ed.). Whitehouse Station, N.J.: Merck.

Ochsner, A., & Augustin, C. (2007). *Multifunctional Metallic Hollow Sphere Structures*: Springer.

Oliveira, B. F., Da Cunda, L. A., Ochsner, A., & Creus, G. J. (2009). Hollow sphere structure: a study of mechanical behaviour using numerical simulation. *Materialwissenschaft und Werkstofftechnik, 40*(3), 144-153.

Rabiei, A., & O'Neill, A. T. (2005). A study on processing of a composite metal foam via casting. *Materials Science and Engineering a-Structural Materials Properties Microstructure and Processing, 404*(1-2), 159-164.

Rabiei, A., & Vendra, L. J. (2009). A comparison of composite metal foam's properties and other comparable metal foams. *Materials Letters, 63*(5), 533-536.

Rachor, L., & Lotz, H. (1966). United States Patent No. 3284314. U. S. P. Office.

Roush, M. S., & Clark, C. C. (1952). United States Patent No. 2609576. U. S. P. Office.

Ruan, D., Lu, G., Chen, F. L., & Siores, E. (2002). Compressive behaviour of aluminium foams at low and medium strain rates. *Composite Structures, 57*(1-4), 331-336.

Sanderow, H. I., & Murphy, T. (2000). *Quantitative Image Analysis Technique for Determining Local density Variation*. Paper presented at the International Conference on Powder Metallurgy and Particulate Materials New York.

Sanders, W. S., & Gibson, L. J. (2003). Mechanics of hollow sphere foams. *Materials Science and Engineering a-Structural Materials Properties Microstructure and Processing, 347*(1-2), 70-85.

Schatz, J. W. (1910). United States Patent No. 955698. U. S. P. Office.

Schlieper, G. (2000). Principles of gamma ray densitometry. *Metal Powder Report*.

Schlieper, G. (2010). Measuring PM density by going outside the visible spectrum. *Metal Powder Report*.

Selig, S. (2012). *Finite Element Simulation of the Compaction and Springback of an Aluminum Powder Metallurgy Alloy*. M.A.Sc., Dalhousie University, Halifax.

Selig, S., & Doman, D. A. (2011a). *Finite Element Simulation of the Compaction and Springback of Aluminum Powder Metallurgy Alloys*. Paper presented at the International Conference on Powder Metallurgy & Particulate Materials, San Francisco.

Selig, S., & Doman, D. A. (2011b). Finite Element Simulation of the Compaction of Aluminum-Base PM Gears. *Internaational Journal of Powder Metallurgy, 47*(4), 9-10.

Seyferth, D., & Czubarow, P. (1995). 5455000. U. S. P. Office.

Sinka, I., Burth, S., Tweed, J., & Cunningham, J. (2004). Measurement of density variations in tablets using X-ray computed tomography. *Internaational Journal of Pharmaceutics*(271), 215-224.

Spahr, O. (1907). United States Patent No. 861403. U. S. P. Office.

Stepanenko, A., Boginskii, L., Girutskii, I., & Pavlovskaya, L. (1984). Dertermination of the Density of Porous Meterials by Gamma Radiography. *Poroshkovaya Metallurgiya*(7), 42-46.

Vesenjak, M., Fiedler, T., Ren, Z., & Ochsner, A. (2008). Behaviour of Syntactic and Parial Hollow Sphere Structures under Dynamic Loading. *Advanced Engineering Materials, 10*(3), 185-191.

Voice, W. E., & Junfa, M. (2008). United States Patent No. 7407622 B2. U. S. P. Office.

Wang, T. G., & Elleman, D. D. (1982). United States Patent No. 4344787. U. S. P. Office.

Watanabe, T., Ohhori, M., Ohta, A., & Kondo, Y. (1981). 4261745. U. S. P. Office.

Weber, G. G., & Brown, S. B. (1989). Simulation of the Compaction of Powder Components. *1989 Advances in Powder Metallurgy, Vols 1-3, 1-3*, A105-A118.

Zhan-you, L., Xian-rong, Z., & Xian-nan, G. (2007). Expansion of spherical cavity of strain-softening materials with different elastic moduli of tension and compression. *Journal of Zhejiang University - Science A, 8*(9), 1380-1387.

APPENDIX A: LS-DYNA CODE FOR INTERNAL STRUCTURES COMPACTION AT 300 MPA

```
$ Units
$---+----1----+----2----+----3----+----4----+----5----+----6----+----7----+----8
$   LENGTH      MASS      TIME     FORCE    STRESS    ENERGY     POWER   DENSITY
$      [m]      [kg]       [s]       [N]      [Pa]       [J]       [W]   [kg/m3]
$
$
*KEYWORD_ID
$---+----1----+----2----+----3----+----4----+----5----+----6----+----7----+----8
$            PROJECT                 NUM                                   STAGE
C3                  PWD_AL3003          008
$
$
$---+----1----+----2----+----3----+----4----+----5----+----6----+----7----+----8
$                                                                             $
$                          PARAMETER DEFINITIONS                              $
$                                                                             $
$---+----1----+----2----+----3----+----4----+----5----+----6----+----7----+----8
*PARAMETER
$---+----1----+----2----+----3----+----4----+----5----+----6----+----7----+----8
$    PRMR1      VAL1     PRMR2      VAL2     PRMR3      VAL3     PRMR4      VAL4
R ENDTIM    +0.04100R HLDTIM    +0.03800R DTOUT      +0.0002R MAXDISP    -0.0150
$    PRMR5      VAL5     PRMR6      VAL6     PRMR7      VAL7     PRMR8      VAL8
R LOAD         -8000R FRIC       +0.2400R SFACT         1.00
$
$
*TITLE
C3 DOUBLE-ACTION 300MPa
$
$
$---+----1----+----2----+----3----+----4----+----5----+----6----+----7----+----8
$                                                                             $
$                                  CONTROL CARD                               $
$                                                                             $
$---+----1----+----2----+----3----+----4----+----5----+----6----+----7----+----8
*CONTROL_TIMESTEP
$---+----1----+----2----+----3----+----4----+----5----+----6----+----7----+----8
$   DTINIT    TSSFAC      ISDO    TSLIMT     DT2MS      LCTM     ERODE     MS1ST
         0       1.0         0       0.0       0.0         0         0         0
$---+----1----+----2
$   DT2MSF   DT2MSLC

$
$
*CONTROL_TERMINATION
$---+----1----+----2----+----3----+----4----+----5
$   ENDTIM    ENDCYC     DTMIN    ENDENG    ENDMAS
&ENDTIM            0       0.0       0.0       0.0
$
$
*CONTROL_ENERGY
$---+----1----+----2----+----3----+----4
$     HGEN      RWEN    SLNTEN     RYLEN
         2         1         2         1
$
$
$*CONTROL_HOURGLASS
$---+----1----+----2
$      IHQ        QH
$         1      0.10
$
$
```

```
$---+----1----+----2----+----3----+----4----+----5----+----6----+----7----+----8
$                                                                              $
$                         DATABASE CONTROL FOR BINARY                          $
$                                                                              $
$---+----1----+----2----+----3----+----4----+----5----+----6----+----7----+----8
*DATABASE_BINARY_D3PLOT
$---+----1----+----2----+----3----+----4
$  DT/CYCL      LCDT      BEAM     NPLTC
&DTOUT             0         0         0
$---+----1
$    IOOPT
         0
$
$
*DATABASE_GLSTAT
$---+----1----+----2----+----3----+----4----+----5----+----6
$       DT    BINARY      LCUR     IOOPT     DTHFF     BINHF
&DTOUT
$
$
*DATABASE_MATSUM
$---+----1----+----2----+----3----+----4----+----5----+----6
$       DT    BINARY      LCUR     IOOPT     DTHFF     BINHF
&DTOUT
$
$
*DATABASE_RCFORC
$---+----1----+----2----+----3----+----4----+----5----+----6
$       DT    BINARY      LCUR     IOOPT     DTHFF     BINHF
&DTOUT
$
*DATABASE_RBDOUT
$---+----1----+----2----+----3----+----4----+----5----+----6
$       DT    BINARY      LCUR     IOOPT     DTHFF     BINHF
&DTOUT
$
$---+----1----+----2----+----3----+----4----+----5----+----6----+----7----+----8
$                                                                              $
$                                  PART CARDS                                  $
$                                                                              $
$---+----1----+----2----+----3----+----4----+----5----+----6----+----7----+----8
$
*INCLUDE
$
ddmesh.k
$
*INCLUDE
matdef.k
$
*INCLUDE
cavity.part
$
*INCLUDE
cavity_shell.part
$
*INCLUDE
powder.part
$
*INCLUDE
die.part
$
*INCLUDE
toppunch.part
$
*INCLUDE
bottompunch.part
$
$---+----1----+----2----+----3----+----4----+----5----+----6----+----7----+----8
$                                                                              $
$                               CONTACT CARDS                                  $
$                                                                              $
```

```
$---+----1----+----2----+----3----+----4----+----5----+----6----+----7----+----8
*SET_PART_LIST_TITLE
$--------------------------------------+---------------------------------------1
$                                                                        HEADING
CAVITY PARTS
$---+----1----+----2----+----3----+----4----+----5
$      SID       DA1       DA2       DA3       DA4
     50001
$---+----1----+----2----+----3----+----4----+----5----+----6----+----7----+----8
$     PID1      PID2      PID3      PID4      PID5      PID6      PID7      PID8
     50001
$
$
*SET_PART_LIST_TITLE
$--------------------------------------+---------------------------------------1
$                                                                        HEADING
CAVITY SHELL PARTS
$---+----1----+----2----+----3----+----4----+----5
$      SID       DA1       DA2       DA3       DA4
     10001
$---+----1----+----2----+----3----+----4----+----5----+----6----+----7----+----8
$     PID1      PID2      PID3      PID4      PID5      PID6      PID7      PID8
     10001
$
$
*SET_PART_LIST_TITLE
$--------------------------------------+---------------------------------------1
$                                                                        HEADING
POWDER PARTS
$---+----1----+----2----+----3----+----4----+----5
$      SID       DA1       DA2       DA3       DA4
    100001
$---+----1----+----2----+----3----+----4----+----5----+----6----+----7----+----8
$     PID1      PID2      PID3      PID4      PID5      PID6      PID7      PID8
    100001
$
*SET_PART_LIST_TITLE
$--------------------------------------+---------------------------------------1
$                                                                        HEADING
DW
$---+----1----+----2----+----3----+----4----+----5
$      SID       DA1       DA2       DA3       DA4
         1
$---+----1----+----2----+----3----+----4----+----5----+----6----+----7----+----8
$     PID1      PID2      PID3      PID4      PID5      PID6      PID7      PID8
         1
$
*SET_PART_LIST_TITLE
$--------------------------------------+---------------------------------------1
$                                                                        HEADING
BP
$---+----1----+----2----+----3----+----4----+----5
$      SID       DA1       DA2       DA3       DA4
         2
$---+----1----+----2----+----3----+----4----+----5----+----6----+----7----+----8
$     PID1      PID2      PID3      PID4      PID5      PID6      PID7      PID8
         2
$
$
*SET_PART_LIST_TITLE
$--------------------------------------+---------------------------------------1
$                                                                        HEADING
TP
$---+----1----+----2----+----3----+----4----+----5
$      SID       DA1       DA2       DA3       DA4
         3
$---+----1----+----2----+----3----+----4----+----5----+----6----+----7----+----8
$     PID1      PID2      PID3      PID4      PID5      PID6      PID7      PID8
         3
$
$
```

```
*CONTACT_2D_AUTOMATIC_SURFACE_TO_SURFACE_ID
$---+----1----------------------------------+---------------------------------2
$      CID                                                            HEADING
         1CAV_PWD
$---+----1----+----2----+----3----+----4----+----5----+----6----+----7----+----8
$     SIDS      SIDM     SFACT      FREQ        FS         FD        DC     MEMBS
    100001     10001&SFACT            50&FRIC
$---+----1----+----2----+----3----+----4----+----5----+----6----+----7----+----8
$   TBIRTH    TDEATH       SOS       SOM       NDS       NDM       COF      INIT
                                                                           1
$
$
*CONTACT_2D_AUTOMATIC_SURFACE_TO_SURFACE_ID
$---+----1----------------------------------+---------------------------------2
$      CID                                                            HEADING
         2                                                  CAVITY SHELL-CAVITY
$---+----1----+----2----+----3----+----4----+----5----+----6----+----7----+----8
$     SIDS      SIDM     SFACT      FREQ        FS         FD        DC     MEMBS
     50001     10001&SFACT            50&FRIC
$---+----1----+----2----+----3----+----4----+----5----+----6----+----7----+----8
$   TBIRTH    TDEATH       SOS       SOM       NDS       NDM       COF      INIT
                                                                           1
$
$
*CONTACT_2D_AUTOMATIC_SURFACE_TO_SURFACE_ID
$---+----1----------------------------------+---------------------------------2
$      CID                                                            HEADING
         3                                                          TP-POWDER
$---+----1----+----2----+----3----+----4----+----5----+----6----+----7----+----8
$     SIDS      SIDM     SFACT      FREQ        FS         FD        DC     MEMBS
    100001        3&SFACT            50&FRIC
$---+----1----+----2----+----3----+----4----+----5----+----6----+----7----+----8
$   TBIRTH    TDEATH       SOS       SOM       NDS       NDM       COF      INIT
                                                                           1
$
$
*CONTACT_2D_AUTOMATIC_SURFACE_TO_SURFACE_ID
$---+----1----------------------------------+---------------------------------2
$      CID                                                            HEADING
         4                                                          BP-POWDER
$---+----1----+----2----+----3----+----4----+----5----+----6----+----7----+----8
$     SIDS      SIDM     SFACT      FREQ        FS         FD        DC     MEMBS
    100001         2&SFACT            50&FRIC
$---+----1----+----2----+----3----+----4----+----5----+----6----+----7----+----8
$   TBIRTH    TDEATH       SOS       SOM       NDS       NDM       COF      INIT
                                                                           1
$
$
*CONTACT_2D_AUTOMATIC_SURFACE_TO_SURFACE_ID
$---+----1----------------------------------+---------------------------------2
$      CID                                                            HEADING
         5                                                          DW-POWDER
$---+----1----+----2----+----3----+----4----+----5----+----6----+----7----+----8
$     SIDS      SIDM     SFACT      FREQ        FS         FD        DC     MEMBS
    100001         1&SFACT            50     0.440
$---+----1----+----2----+----3----+----4----+----5----+----6----+----7----+----8
$   TBIRTH    TDEATH       SOS       SOM       NDS       NDM       COF      INIT
                                                                           1
$
$
$---+----1----+----2----+----3----+----4----+----5----+----6----+----7----+----8
$                                                                          $
$                           MOTION/DYNAMICS CARDS                          $
$                                                                          $
$---+----1----+----2----+----3----+----4----+----5----+----6----+----7----+----8
$*LOAD_RIGID_BODY
$---+----1----+----2----+----3----+----4----+----5----+----6----+----7----+----8
$      PID       DOF      LCID        SF       CID        M1        M2        M3
$         3         2         1&LOAD
$
$
```

```
*BOUNDARY_PRESCRIBED_MOTION_RIGID
$---+----1----+----2----+----3----+----4----+----5----+----6----+----7----+----8
$      PID       DOF       VAD      LCID        SF       VID     DEATH     BIRTH
         3         2         2         2      1.00
$
$
$---+----1----+----2----+----3----+----4----+----5----+----6----+----7----+----8
$                                                                               $
$                              LOAD CURVE CARDS                                 $
$                                                                               $
$---+----1----+----2----+----3----+----4----+----5----+----6----+----7----+----8
$
$
*DEFINE_CURVE
$---+----1----+----2----+----3----+----4----+----5----+----6----+----7
$     LCID      SIDR       SFA       SFO      OFFA      OFFO    DATTYP
         2         0      +1.0      +1.0       0.0       0.0         0
$---+----1----+----2----+----3----+----4
$            XVALUES             YVALUES
$            XVALUES             YVALUES
               0.000            -0.00000
               0.004            -0.00147
               0.008            -0.00294
               0.012            -0.00441
               0.016            -0.00588
               0.020            -0.00735
               0.024            -0.00882
               0.028            -0.01029
               0.032            -0.01179
               0.036            -0.01323
               0.040            -0.01470
               0.100            -0.01470
$
$
*END
```

Matdef.k

```
*KEYWORD
$
$---+----1----+----2----+----3----+----4----+----5----+----6----+----7----+----8
$                                                                               $
$                           STEEL MATERIAL MODELS                               $
$                                                                               $
$---+----1----+----2----+----3----+----4----+----5----+----6----+----7----+----8
*MAT_RIGID_TITLE
$---+----1
$  HEADING
STEEL,DIE
$---+----1----+----2----+----3----+----4----+----5----+----6----+----7----+----8
$      MID        RO         E        PR         N    COUPLE         M     ALIAS
       ST1      7800 210.0E+09      0.29
$---+----1----+----2----+----3
$      CMO      CON1      CON2
      +1.0       7.0       7.0
$---+----1----+----2----+----3----+----4----+----5----+----6
$   LCO/A1        A2        A3        V1        V2        V3

$
*MAT_RIGID_TITLE
$---+----1
$  HEADING
STEEL,DIE
$---+----1----+----2----+----3----+----4----+----5----+----6----+----7----+----8
$      MID        RO         E        PR         N    COUPLE         M     ALIAS
       ST2      7800 210.0E+09      0.29
$---+----1----+----2----+----3
$      CMO      CON1      CON2
```

```
      +1.0       6.0       7.0
$---+----1----+----2----+----3----+----4----+----5----+----6
$   LCO/A1        A2        A3        V1        V2        V3

$
$
*MAT_GEOLOGIC_CAP_MODEL_TITLE
$ S. Selig - February 29, 2012
$ THEORETICAL MAX DENSITY = 2780 KG/M3
$ RO - 44.7% of max density BULK and G - 44.7% of values from matweb? GAMMA and BETA = 0?
TOFF = ???
$---+----1
$  HEADING
ALUMIX 321
$---+----1----+----2----+----3----+----4----+----5----+----6----+----7----+----8
$      MID        RO      BULK         G     ALPHA     THETA     GAMMA      BETA
       PW2      1243  48.87E+9  11.62E+9         0     0.394         0         0
$---+----1----+----2----+----3----+----4----+----5----+----6
$        R         D         W        X0         C         N
     2.800   1.4e-09      0.76
$---+----1----+----2----+----3----+----4
$     PLOT     FTYPE       VEC      TOFF
       3.0       1.0       0.0 -2.068E+6
$
$
$
*MAT_SIMPLIFIED_JOHNSON_COOK_TITLE
$---+----1
$  HEADING
$Kay (2003)
ALUMINUM
$---+----1----+----2----+----3----+----4----+----5
$      MID        RO         E        PR        VP
       AL6      2780  73.1E+09      0.29
$
$---+----1----+----2----+----3----+----4----+----5----+----6----+----7----+----8
$        A         B         N         C    PSFAIL    SIGMAX    SIGSAT      EPSO
  3.52E+08   4.4E+08      0.42    0.0083
$
$
*MAT_SOIL_AND_FOAM
$---+----1----+----2----+----3----+----4----+----5----+----6----+----7----+----8
$      MID        RO         G         K        A0        A1        A2        PC
        X7     954.0  4.929E10 2.300E+11   1.33E16         0         0         0
$---+----1----+----2
$      VCR       REF
       1.0         0
$---+----1----+----2----+----3----+----4----+----5----+----6----+----7----+----8
$     EPS1      EPS2      EPS3      EPS4
         0     0.100     0.500     0.900
$---+----1----+----2
$     EPS9     EPS10

$---+----1----+----2----+----3----+----4----+----5----+----6----+----7----+----8
$       P1        P2        P3        P4
         0 +225.0E06 +350.0E06 +1.000E09
$---+----1----+----2----+----3----+----4----+----5----+----6----+----7----+----8
$       P9       P10

$
$
*END
```

Powder.part

```
*PART
$--------------------------------------+----------------------------------------1
$                                                                        HEADING
```

```
POWDER
$---+----1----+----2----+----3----+----4----+----5----+----6----+----7----+----8
$       PID     SECID       MID     EOSID      HGID      GRAV    ADPOPT      TMID
    100001    100001       PW2         0         0         0         0         0
$
$
$---+----1----+----2----+----3----+----4----+----5----+----6----+----7----+----8
$                                                                               $
$                              SECTION KEYWORDS                                 $
$                                                                               $
$---+----1----+----2----+----3----+----4----+----5----+----6----+----7----+----8
*SECTION_SHELL_TITLE
$-------------------------------------+---------------------------------------1
$                                                                       HEADING
AXISYMMETRIC SHELL
$---+----1----+----2----+----3----+----4----+----5----+----6----+----7----+----8
$    SECID    ELFORM      SHRF       NIP     PROPT   QR/IRID     ICOMP     SETYP
    100001        15       1.0         2       0.0       0.0         0         1
$
$---+----1----+----2----+----3----+----4----+----5----+----6----+----7----+----8
$       T1        T2        T3        T4      NLOC     MAREA      IDOF    EDGSET
       0.0       0.0       0.0       0.0       0.0       0.0       0.0
$
$
*END
```

Toppunch.part

```
*PART
$---+----1
$  HEADING
TOPPUNCH
$---+----1----+----2----+----3----+----4----+----5----+----6----+----7----+----8
$       PID     SECID       MID     EOSID      HGID      GRAV    ADPOPT      TMID
          3         3       ST2         0         0         0         0         0
$
$
$---+----1----+----2----+----3----+----4----+----5----+----6----+----7----+----8
$                                                                               $
$                              SECTION KEYWORDS                                 $
$                                                                               $
$---+----1----+----2----+----3----+----4----+----5----+----6----+----7----+----8
*SECTION_SHELL
$---+----1
$  HEADING
$SOLID, PUNCH
$---+----1----+----2----+----3----+----4----+----5----+----6----+----7----+----8
$    SECID    ELFORM      SHRF       NIP     PROPT   QR/IRID     ICOMP     SETYP
          3        15       1.0         2       0.0       0.0         0         1
$
$---+----1----+----2----+----3----+----4----+----5----+----6----+----7----+----8
$       T1        T2        T3        T4      NLOC     MAREA      IDOF    EDGSET
       0.0       0.0       0.0       0.0       0.0       0.0       0.0
$
$
*END
```

Bottompunch.part

```
*PART
$---+----1
$  HEADING
TOPPUNCH
$---+----1----+----2----+----3----+----4----+----5----+----6----+----7----+----8
$       PID     SECID       MID     EOSID      HGID      GRAV    ADPOPT      TMID
```

```
         2         2       ST1         0         0         0         0         0
$
$
$---+----1----+----2----+----3----+----4----+----5----+----6----+----7----+----8
$                                                                               $
$                              SECTION KEYWORDS                                 $
$                                                                               $
$---+----1----+----2----+----3----+----4----+----5----+----6----+----7----+----8
*SECTION_SHELL
$---+----1
$  HEADING
$SOLID, PUNCH
$---+----1----+----2----+----3----+----4----+----5----+----6----+----7----+----8
$    SECID    ELFORM      SHRF       NIP     PROPT   QR/IRID     ICOMP     SETYP
         2        15       1.0         2       0.0       0.0         0         1
$
$---+----1----+----2----+----3----+----4----+----5----+----6----+----7----+----8
$       T1        T2        T3        T4      NLOC     MAREA      IDOF    EDGSET
       0.0       0.0       0.0       0.0       0.0       0.0       0.0
$
$
*END
```

Die.part

```
*PART
$---+----1
$  HEADING
DIE
$---+----1----+----2----+----3----+----4----+----5----+----6----+----7----+----8
$      PID     SECID       MID     EOSID      HGID      GRAV    ADPOPT      TMID
         1         1       ST1         0         0         0         0         0
$
$
$---+----1----+----2----+----3----+----4----+----5----+----6----+----7----+----8
$                                                                               $
$                              SECTION KEYWORDS                                 $
$                                                                               $
$---+----1----+----2----+----3----+----4----+----5----+----6----+----7----+----8
*SECTION_SHELL
$---+----1
$  HEADING
$SOLID, DIE
$---+----1----+----2----+----3----+----4----+----5----+----6----+----7----+----8
$    SECID    ELFORM      SHRF       NIP     PROPT   QR/IRID     ICOMP     SETYP
         1        15       1.0         2       0.0       0.0         0         1
$
$---+----1----+----2----+----3----+----4----+----5----+----6----+----7----+----8
$       T1        T2        T3        T4      NLOC     MAREA      IDOF    EDGSET
       0.0       0.0       0.0       0.0       0.0       0.0       0.0
$
*END
```

Cavity.part

```
*PART
$---------------------------------------+---------------------------------------1
$                                                                       HEADING
CAVITY
$---+----1----+----2----+----3----+----4----+----5----+----6----+----7----+----8
$      PID     SECID       MID     EOSID      HGID      GRAV    ADPOPT      TMID
     50001     50001        X7
$
$
*HOURGLASS
```

```
$---+----1----+----2----+----3----+----4----+----5----+----6----+----7----+----8
$     HGID       IHQ        QM       IBQ        Q1        Q2    QB/VDC        QW
     50001         6      0.14
$
$
$---+----1----+----2----+----3----+----4----+----5----+----6----+----7----+----8
$                                                                               $
$                              SECTION KEYWORDS                                 $
$                                                                               $
$---+----1----+----2----+----3----+----4----+----5----+----6----+----7----+----8
*SECTION_SHELL_TITLE
$---------------------------------------+---------------------------------------1
$                                                                       HEADING
AXISYMMETRIC SHELL
$---+----1----+----2----+----3----+----4----+----5----+----6----+----7----+----8
$    SECID    ELFORM      SHRF       NIP     PROPT   QR/IRID     ICOMP     SETYP
     50001        15       1.0         2       0.0       0.0         0         1
$
$---+----1----+----2----+----3----+----4----+----5----+----6----+----7----+----8
$       T1        T2        T3        T4      NLOC     MAREA      IDOF    EDGSET
       0.0       0.0       0.0       0.0       0.0       0.0       0.0
$
$
*END
```

Cavityshell.part

```
*PART
$---------------------------------------+---------------------------------------1
$                                                                       HEADING
CAVITY SHELL
$---+----1----+----2----+----3----+----4----+----5----+----6----+----7----+----8
$      PID     SECID       MID     EOSID      HGID      GRAV    ADPOPT      TMID
     10001     10001       AL6         0     10001         0         0         0
$
$
*HOURGLASS
$---+----1----+----2----+----3----+----4----+----5----+----6----+----7----+----8
$     HGID       IHQ        QM       IBQ        Q1        Q2    QB/VDC        QW
     10001         6      0.14
$
$
$---+----1----+----2----+----3----+----4----+----5----+----6----+----7----+----8
$                                                                               $
$                              SECTION KEYWORDS                                 $
$                                                                               $
$---+----1----+----2----+----3----+----4----+----5----+----6----+----7----+----8
*SECTION_SHELL_TITLE
$---------------------------------------+---------------------------------------1
$                                                                       HEADING
AXISYMMETRIC SHELL
$---+----1----+----2----+----3----+----4----+----5----+----6----+----7----+----8
$    SECID    ELFORM      SHRF       NIP     PROPT   QR/IRID     ICOMP     SETYP
     10001        15       1.0         2       0.0       0.0         0         1
$
$---+----1----+----2----+----3----+----4----+----5----+----6----+----7----+----8
$       T1        T2        T3        T4      NLOC     MAREA      IDOF    EDGSET
       0.0       0.0       0.0       0.0       0.0       0.0       0.0
$
$
*END
```

APPENDIX B: COMPACTION CURVE DATA

Conventional Samples

Compaction Pressure (MPa)	Fill Height (mm)	Height (mm)	Diameter (mm)	Mass (g)	Density (g/cc)	STDEV (g/cc)	Average Density
100	30.34	17.437	15.081	6.652	2.136	N/A	N/A
100	29.72	17.348	15.095	6.643	2.140	N/A	N/A
100	30.32	17.432	15.095	6.646	2.130	N/A	N/A
100	30.13	17.360	15.096	6.648	2.140	N/A	N/A
100	30.16	17.340	15.096	6.644	2.141	0.004	2.137
200	30.38	15.229	15.092	6.640	2.437	N/A	N/A
200	30.32	15.310	15.091	6.646	2.427	N/A	N/A
200	30.34	15.300	15.091	6.646	2.429	N/A	N/A
200	30.44	15.303	15.086	6.649	2.431	N/A	N/A
200	30.43	15.303	15.088	6.646	2.429	0.004	2.431
300	30.48	14.757	15.090	6.644	2.517	N/A	N/A
300	30.41	14.745	15.076	6.643	2.524	N/A	N/A
300	30.60	14.747	15.086	6.645	2.521	N/A	N/A
300	30.38	14.757	15.078	6.644	2.521	N/A	N/A
300	30.48	14.759	15.090	6.645	2.518	0.003	2.520
400	30.17	14.541	15.084	6.640	2.555	N/A	N/A
400	30.33	14.554	15.083	6.639	2.553	N/A	N/A
400	30.23	14.573	15.081	6.638	2.550	N/A	N/A
400	29.96	14.607	15.085	6.637	2.542	N/A	N/A
400	30.29	14.550	15.076	6.626	2.551	0.005	2.550

Internal Structures Samples

Compaction Pressure (MPa)	Fill Height (mm)	Height (mm)	Diameter (mm)	Mass (g)	Density (g/cc)	STDEV (g/cc)	Average Density
100	29.58	17.135	15.095	6.503	2.121	N/A	N/A
100	29.29	17.193	15.097	6.502	2.113	N/A	N/A
100	29.30	17.204	15.095	6.501	2.112	N/A	N/A
100	29.61	17.317	15.103	6.503	2.096	N/A	N/A
100	29.26	17.279	15.095	6.496	2.101	0.010	2.108
200	29.35	15.291	15.097	6.499	2.374	N/A	N/A
200	29.54	15.253	15.096	6.500	2.381	N/A	N/A
200	29.52	15.259	15.093	6.501	2.381	N/A	N/A
200	29.38	15.293	15.093	6.498	2.375	N/A	N/A
200	29.52	15.298	15.086	6.500	2.377	0.003	2.378
300	28.84	14.729	15.102	6.485	2.458	N/A	N/A
300	29.21	14.740	15.095	6.492	2.461	N/A	N/A
300	29.32	14.755	15.107	6.493	2.455	N/A	N/A
300	29.49	14.746	15.097	6.498	2.462	N/A	N/A
300	29.42	14.762	15.091	6.485	2.456	0.003	2.458
400	29.45	14.561	15.089	6.494	2.494	N/A	N/A
400	29.23	14.539	15.086	6.482	2.494	N/A	N/A
400	29.47	14.552	15.080	6.490	2.497	N/A	N/A
400	29.27	14.553	15.083	6.485	2.494	N/A	N/A
400	29.24	14.539	15.077	6.488	2.500	0.002	2.496

APPENDIX C: COMPRESSIVE GREEN STRENGTH DATA

Conventional Samples

Compaction Pressure (MPa)	GS Force (kN)	GS Force (MPa)	STDEV (MPa)	Average CGS (MPa)
100	6.110	34.576	N/A	N/A
100	6.470	36.613	N/A	N/A
100	5.730	32.425	1.710	34.538
200	10.330	58.456	N/A	N/A
200	10.120	57.267	N/A	N/A
200	10.930	61.851	1.942	59.191
300	12.300	69.604	N/A	N/A
300	13.200	74.697	N/A	N/A
300	12.350	69.887	2.337	71.396
400	13.070	73.961	N/A	N/A
400	13.420	75.942	N/A	N/A
400	14.270	80.752	2.851	76.885

Internal Structures Samples

Compaction Pressure (MPa)	YGS Force (kN)	UGS Force (kN)	STDEV (MPa)	Average CGS (MPa)
100	5.180	29.313	N/A	N/A
100	5.530	31.293	N/A	N/A
100	5.044	28.543	1.158	29.716
200	9.170	51.892	N/A	N/A
200	9.430	53.363	N/A	N/A
200	9.960	56.362	1.860	53.872
300	11.650	65.926	N/A	N/A
300	11.460	64.850	N/A	N/A
300	11.010	62.304	1.519	64.360
400	10.550	59.701	N/A	N/A
400	11.870	67.170	N/A	N/A
400	11.260	63.719	3.052	63.530

APPENDIX D: ALUMIX 321 SINTER PROFILE